FOSSEE Winter Internship Report

On

Industrial Engineering Research Projects

Submitted by Shubham Dombale
3rd Year, Department of Computer Engineering
Vidyalankar Institute of Technology, Mumbai

Under the Guidance of
Prof. Jayendran Venkateswaran
Department of IEOR
Indian Institute of Technology Bombay

February 2026

Acknowledgments

I would like to express my sincere gratitude to everyone who supported and guided me throughout the course of my internship and the successful completion of this project. Their encouragement, mentorship, and constructive feedback were instrumental in shaping my learning experience and strengthening my technical understanding.

I am deeply thankful to the **FOSSEE (Free/Libre and Open Source Software for Education)** team for providing me with this valuable opportunity to work on industrial engineering research projects. The internship offered a highly enriching environment that allowed me to apply theoretical knowledge to practical engineering challenges.

I would like to express my sincere appreciation to **Prof. Jayendran Venkateswaran**, **Department of IEOR**, **Indian Institute of Technology Bombay**, for his continuous guidance, mentorship, and technical insights throughout the internship. His direction helped me approach problems with structured engineering thinking and clarity.

I am also grateful to the **M.Tech mentors** who worked closely with me during the internship. Their technical discussions, suggestions, and feedback significantly contributed to the successful completion of the projects.

I would further like to thank **Mr.Sumanto Kar** for his support and coordination during the internship period. His guidance and encouragement played an important role in ensuring smooth progress throughout the internship.

I gratefully acknowledge the support of the **National Mission on Education through Information and Communication Technology (ICT)**, **Ministry of Education (MoE)**, **Government of India**, for facilitating this project and enabling such valuable learning opportunities.

Finally, I extend my sincere thanks to my institution, **Vidyalankar Institute of Technology**, and its faculty members for their continued encouragement and support.

Contents

Chapter 1

Introduction

1.1 National Mission on Education through ICT

The National Mission on Education through ICT (NMEICT) is a centrally sponsored scheme under the Department of Higher Education, Ministry of Education (MoE), Government of India. It was established to leverage the transformative potential of Information and Communication Technology (ICT) to enhance teaching and learning processes across Higher Education Institutions. The mission operates on an anytime-anywhere learning paradigm and aligns strictly with the three cardinal principles of the National Education Policy: access, equity, and quality.

To achieve these goals, the mission focuses on two major components: providing affordable access devices and connectivity to all learners and institutions, and generating high-quality e-content free of cost. NMEICT aims to seamlessly bridge the digital divide, ensuring that students and teachers in both urban and rural areas are empowered to participate in the modern knowledge economy. Its key focus areas include the development of e-learning pedagogies, the establishment of virtual laboratories, and the facilitation of online testing and certification through accessible platforms like EduSAT and Direct-to-Home (DTH) networks. Furthermore, it heavily emphasizes training teachers to integrate ICT-based methodologies into their traditional teaching frameworks. For more details, the official portal is accessible at www.nmeict.ac.in.

1.1.1 ICT Initiatives of the Ministry of Education

Under the NMEICT umbrella, the Ministry of Education has launched numerous specialized initiatives targeting students, researchers, and academic institutions. Rather than relying on physical infrastructure alone, these initiatives provide scalable digital resources:

- **SWAYAM & SWAYAMPRABHA:** SWAYAM allows students to earn academic credits via structured online courses, while institutions can host these courses and accept the credits. SWAYAMPRABHA complements this by broadcasting 24x7 educational TV programs for continuous learning.
- **National Digital Library (NDL) & e-PG Pathshala:** These platforms provide vast repositories of e-content across multiple disciplines. Students gain free access to textbooks and full-text e-resources, while institutions can list their e-content and form NDL Clubs.
- **Shodhganga & e-ShodhSindhu:** Aimed directly at the research community, Shodhganga provides access to Indian research theses, and e-ShodhSindhu provides institutional access to vital e-resources.
- **Hands-on Learning Platforms:** Initiatives like **e-Yantra** provide hands-on training in embedded systems, allowing institutions to create dedicated labs in collaboration with IIT Bombay. Similarly, **Virtual Labs** allow students to perform curriculum-based online experiments without needing physical lab equipment.
- **FOSSEE & Spoken Tutorial:** These initiatives promote self-learning of IT skills and encourage volunteering for open-source software development. They empower institutions to run modern technical labs without the financial burden of proprietary software licenses.

1.2 The FOSSEE Project

The FOSSEE (Free/Libre and Open Source Software for Education) project is a flagship initiative specifically designed to promote the use of open-source tools in academia and research. Sponsored by the NMEICT and the Ministry of Education, FOSSEE aims to reduce the dependency of Indian educational institutions on expensive, proprietary software.

1.2.1 Projects and Core Activities

FOSSEE supports the widespread adoption of various open-source alternatives to enhance the quality of technical education. Its core activities are divided into several strategic areas:

- **Textbook Companion Project:** FOSSEE volunteers port solved examples from standard engineering and science textbooks into open-source software environments, creating a massive repository of accessible reference material.
- **Lab Migration:** The project actively facilitates and guides institutions in migrating their existing proprietary software labs to Free/Libre and Open Source Software (FLOSS) alternatives.
- **Niche Software Promotion:** FOSSEE undertakes specialized campaigns to promote highly specific, niche software tools that are critical for advanced engineering research but are traditionally locked behind expensive licenses.
- **Community Building:** FOSSEE hosts user forums and organizes regular workshops and conferences to train students and faculty, fostering a collaborative, self-sustaining ecosystem of open-source developers and users.

1.2.2 Fellowships and Internships

To drive continuous engagement, FOSSEE offers various competitive internship and fellowship opportunities, including the Winter Internship, Summer Fellowship, and Semester-Long Internships.

These programs are uniquely accessible; students from any degree background and academic stage are eligible to apply. The selection process is strictly merit-based, relying on the completion of rigorous screening tasks. These tasks typically involve programming, scientific computing, or data collection exercises designed to directly benefit the broader FLOSS community. Candidates are expected to complete these tasks within a tight one-week timeframe, testing both their technical proficiency and their ability to deliver under pressure. Further information regarding these opportunities is maintained on the official FOSSEE website.

Chapter 2

Internship Project 1: Automated Guided Vehicle (AGV)

2.1 Introduction to Automated Guided Vehicles

The advent of **Industry 4.0** has necessitated a radical shift in material handling, warehousing, and manufacturing logistics. At the core of this transition is the **Automated Guided Vehicle (AGV)**. An AGV is a portable, computer-controlled, and wheel-based load carrier that navigates along the floor of a facility without an onboard operator or driver. Their primary function is to transport heavy materials, WIP (Work-in-Progress) assemblies, and finished goods across industrial floors predictably, safely, and efficiently. By replacing traditional, human-operated forklifts and conveyor systems, AGVs significantly reduce labor costs, minimize workplace accidents, and allow for highly flexible, modular manufacturing layouts.

2.2 Historical Background and Evolution

The conceptualization and deployment of the first Automated Guided Vehicle date back to **1953**. It was developed by **Barrett Electronics Corporation**, a company led by inventor **A.M. Barrett Jr.** The first iteration was simply a modified towing tractor that followed a wire placed in a shallow trench in the facility floor. This wire emitted a magnetic field, which the vehicle's rudimentary sensors tracked. This invention revolutionized material

handling, leading to **Barrett Electronics** being widely recognized as the pioneer of the AGV industry.

Through the 1970s, the technology evolved. The introduction of solid-state electronics allowed AGVs to become more compact and reliable. During this era, **Volvo** pioneered the use of AGVs as mobile assembly platforms in their **Kalmar, Sweden** automotive plant. Instead of a traditional moving assembly line, individual car chassis were placed on custom AGVs, which moved autonomously from workstation to workstation.

The 1980s and 1990s saw the introduction of laser-guided vehicles and the implementation of microprocessors, which allowed for complex dispatching and traffic control algorithms. Today, the lineage of **A.M. Barrett's** invention has culminated in highly advanced robotics utilizing **Artificial Intelligence (AI)** and **Simultaneous Localization and Mapping (SLAM)** to navigate completely infrastructure-free environments.

2.3 Core Components of an AGV System

A modern industrial AGV is a complex integration of mechanical, electrical, and software engineering. The core components include:

- **Chassis and Mechanical Framework:** The structural foundation of the vehicle, typically constructed from welded steel or heavy-duty sheet metal. It must be engineered to withstand immense payload stresses while maintaining a low center of gravity to prevent tipping during maneuvers.
- **Propulsion and Actuation System:** Consists of industrial-grade electric motors (such as high-torque stepper motors or brushless DC motors), gearboxes, and the drive wheels. The propulsion system must be capable of overcoming static friction under maximum payload while providing precise velocity control.
- **Navigation and Sensory Array:** The eyes and ears of the vehicle. This includes the primary navigation sensors (like **LiDAR** or magnetic readers) and safety sensors (such as ultrasonic obstacle detectors, physical bumper switches, and emergency stop mechanisms).
- **Energy Storage and Power Management:** Industrial AGVs typically rely on high-capacity lead-acid, lithium-ion, or LiFePO4 battery banks. Advanced models feature autonomous charging capabilities, allowing the vehicle to navigate to a charging docking station when its voltage drops below a critical threshold.

- **Onboard Supervisory Controller:** The processing brain of the vehicle. Microcontrollers or industrial PCs continuously process sensor data, execute kinematic mathematics (like **PID control**), and regulate motor drivers.

2.4 Classification of AGVs

Automated Guided Vehicles are not universally standardized; they are highly specialized based on their intended industrial application. The primary classifications include:

2.4.1 Tow Vehicles (Tuggers)

These were the first types of AGVs introduced. They are used to pull one or more non-powered trailers, similar to a train. They are capable of moving vast amounts of weight per trip, making them highly efficient for transporting bulk raw materials from a warehouse to a production line.

2.4.2 Unit Load Carriers

These AGVs are equipped with a deck that allows them to carry a discrete load (like a single large engine block or a heavy bin of parts) directly on top of the vehicle. The deck often features integrated mechanisms, such as a localized conveyor belt or a lift table, to automatically transfer the load to a stationary workstation.

2.4.3 Automated Forklifts

Designed to completely replace human-driven forklifts, these vehicles feature automated masts and forks. They are utilized in high-density warehouses to retrieve and place pallets onto multi-level storage racks.

2.4.4 Custom Assembly AGVs

Used heavily in the automotive and aerospace sectors, these are custom-built platforms designed to carry a product through various stages of its assembly. They effectively act as a decentralized, mobile assembly line.

2.5 Navigation and Pathfinding Technologies

The method an AGV uses to navigate defines its flexibility and installation cost. The technologies range from fixed-path to highly dynamic systems:

- **Magnetic Tape and Wire Guidance:** The oldest and most robust method. The AGV uses magnetic sensors to follow a physical magnetic tape adhered to the floor or a current-carrying wire embedded in the concrete. While highly reliable and computationally simple, changing the vehicle's path requires physically altering the facility floor.
- **Laser Target Navigation:** Reflective targets are mounted on walls and columns throughout the facility. The AGV features a rotating laser scanner that continuously bounces light off these targets. By calculating the angle and distance to at least three targets, the AGV uses triangulation to determine its exact coordinates.
- **Vision-Based Navigation:** The AGV uses stereoscopic cameras and advanced computer vision algorithms (such as **OpenCV**) to visually recognize its environment. It follows painted lines on the floor or uses environmental markers.
- **Natural Feature SLAM: Simultaneous Localization and Mapping (SLAM)** is the cutting edge of AGV navigation. Using 2D or 3D **LiDAR**, the AGV actively maps the environment and dynamically plans its path around permanent structures and temporary obstacles without needing any external infrastructure like tape or reflectors.

2.6 Phase 1: Initial Prototype Development

Before committing to heavy industrial materials and complex mechanical fabrication, a scaled-down rapid prototype was constructed. The primary objective of this phase was to validate the core electronics architecture, test the dual-mode software logic (teleoperation versus autonomous tracking), establish a baseline for sensor calibration, and implement fault-tolerant recovery algorithms.

2.6.1 Hardware Architecture and Component Integration

The prototype was built upon a lightweight, planar rapid-prototyping chassis. The component selection was strictly driven by the need for modularity, footprint reduction, and specific input/output (I/O) pin availability. The core hardware architecture consisted of the following interconnected subsystems:

- **Microcontroller Processing Unit (Arduino Nano):** The central brain of the prototype. While the Arduino Uno is standard for basic academic projects, the Nano was specifically selected for two critical engineering reasons. First, its DIP (Dual In-line Package) form factor allowed it to be mounted directly onto a mini breadboard, drastically reducing wiring complexity and signal interference. Second, the Nano's ATmega328P chip exposes 8 Analog-to-Digital Converter (ADC) pins (A0–A7), whereas the Uno only exposes 6. This full 8-pin availability was strictly necessary to interface with the high-resolution 8-channel analog IR sensor array.

- **Propulsion and Actuation System:** The mechanical drive relied on two N20 micro metal gear motors, coupled with 5cm diameter high-traction rubber tires. The N20 motors were chosen for their excellent torque-to-size ratio and precise low-RPM handling, providing sufficient pulling power for the lightweight chassis without drawing excessive stall currents that could brown-out the microcontroller.

- **Motor Driver (L298N H-Bridge):** A standard L298N dual H-bridge motor driver was implemented to manage the high-current demands of the N20 motors. It allowed the microcontroller to control the direction of the motors via logic pins (IN1 through IN4) and modulate their speed via Pulse Width Modulation (PWM) signals sent to the enable pins (ENA and ENB).

- **Navigation Sensor Array:** An 8-channel analog Infrared (IR) sensor array was mounted at the leading edge of the chassis, facing downward. Unlike basic digital IR sensors that use internal comparators to output a binary HIGH/LOW, these analog sensors provided a continuous gradient voltage drop based on the reflectivity of the floor. This allowed the system to calculate the exact geometric center of the black tracking line against a high-reflectance white background.

- **Power Distribution Network:** The system was powered by a customized, high-density battery pack consisting of three 18650 Lithium-Ion cells connected in series. This provided a nominal voltage of 11.1V (peaking at 12.6V fully charged). This raw voltage was routed directly into the L298N motor driver to power the motors, while simultaneously being stepped down by the Arduino Nano's onboard voltage regulator via the VIN pin to provide a stable 5V logic supply for the sensors and receivers.

2.6.2 Dual-Mode Operational Logic

To simulate the varying requirements of an industrial environment—where an autonomous vehicle might need to be manually overridden by a floor operator during an emergency or custom docking procedure—the prototype's firmware was designed with a dual-mode operational architecture.

1. Teleoperation (Manual Control) Mode

For manual override, an Infrared (IR) receiver module (VS1838B) was integrated into the breadboard circuitry. The firmware utilized the NEC communication protocol to decode hex signals transmitted from a standard handheld IR remote control. This allowed an operator to wirelessly dictate the vehicle's kinematic movements. The software mapped the decoded IR hex values to specific kinematic states:

- **Forward/Reverse:** Both motors driven synchronously in the corresponding direction.

- **Differential Turning:** Driving one motor forward while halting the other, allowing for sweeping turns.

- **Pivot Turning:** Driving the left and right motors in opposite directions for zero-radius on-the-spot rotation.

Figure 2.1: Close-up view of the handheld IR remote control used for manual teleoperation, alongside the prototype's breadboard-mounted Arduino Nano and L298N motor driver.

2. Autonomous Line-Following Mode

When commanded to switch to autonomous mode, the system bypassed the IR remote polling loop and dedicated the microcontroller's processing cycles entirely to navigation. The Arduino Nano continuously polled the ADC pins (A0 through A7) at a high refresh rate. Because these sensors are analog, they provided a continuous voltage gradient rather than a simple binary (HIGH/LOW) signal. By evaluating these analog readings, the algorithm calculated a weighted average to determine the exact geometric position of the dark tape relative to the vehicle's center-line, generating a precise, real-time positional error value.

Relying solely on this raw positional error to steer the vehicle typically results in aggressive, unstable oscillations—a phenomenon commonly known as "hunting," where the robot violently zig-zags across the path. To achieve smooth, industrial-grade tracking, the foundational concepts of a **Proportional-Integral-Derivative (PID) control algorithm** were introduced into the autonomous logic.

In basic conceptual terms, the PID controller continuously computes a steering adjustment based on three components:

- **Proportional (P):** Provides an immediate steering response that is directly proportional to the current positional error.
- **Integral (I):** Accumulates past errors over time to correct any persistent, systematic mechanical drift.
- **Derivative (D):** Predicts future error trends, acting as a critical dampener to prevent the vehicle from overshooting the line on sharp curves.

By summing these three terms, the algorithm generates a dynamic control variable that smoothly modulates the PWM duty cycle of the left and right N20 motors. A comprehensive mathematical breakdown of the PID kinematics, the empirical tuning of the constants (K_p, K_i, K_d), and the explicit software implementation will be detailed extensively in the dedicated **Software Implementation and Code** section later in this report.

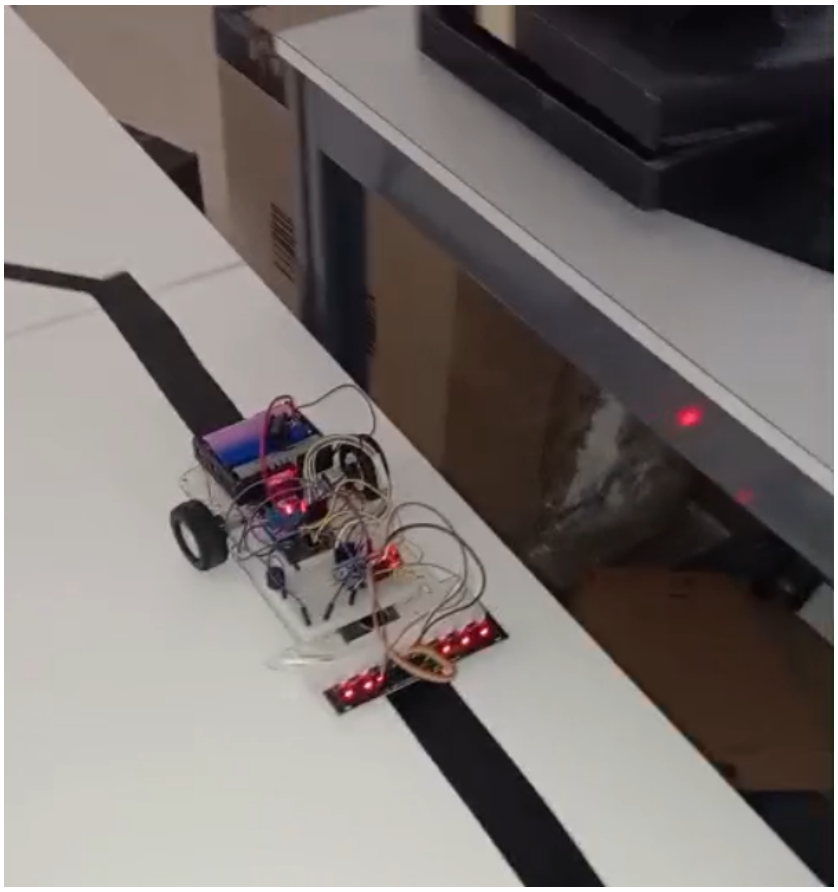

Figure 2.2: The Phase 1 prototype operating in autonomous line-following mode, utilizing the front-mounted 8-channel analog IR array to track the dark path against a high-contrast surface.

2.6.3 Fault-Tolerance: Autonomous Line Recovery Algorithm

One of the most critical features developed during Phase 1 was an autonomous fault-recovery mechanism. In an industrial setting, minor debris, scuffed tape, or sharp angular turns can cause an AGV to momentarily lose

its tracking line. Instead of requiring a human operator to physically reset the vehicle, a recovery algorithm was implemented.

The microcontroller continuously monitored the aggregate values of the 8-channel sensor array. If the system detected a total loss of the line (defined as all 8 sensors returning values consistent with the high-reflectance white floor for a sustained number of clock cycles), it triggered the **Line Recovery Protocol**:

1. **Immediate Halt:** Forward momentum is immediately killed to prevent the vehicle from straying further off the intended path.
2. **360-Degree Search Sweep:** The microcontroller commands the L298N driver to execute a zero-radius pivot turn (left wheels driving in reverse, right wheels driving forward) at a reduced PWM speed.
3. **Dynamic Re-acquisition:** As the vehicle rotates, the sensor array continuously scans the floor. Once the central IR sensors detect a sharp drop in reflectance (indicating the black line has been found), a hardware interrupt-style logic breaks the rotation loop.
4. **Resumption of Transit:** The vehicle realigns itself and resumes standard forward autonomous tracking.

2.6.4 Acoustic Diagnostic Feedback System

In a noisy industrial setting, visual diagnostic LEDs are often insufficient. To provide immediate, auditory machine-state feedback without requiring a wired Serial Monitor connection, a passive buzzer was integrated into the Nano's digital outputs.

The passive buzzer was driven by generating specific PWM frequencies, serving a dual purpose:

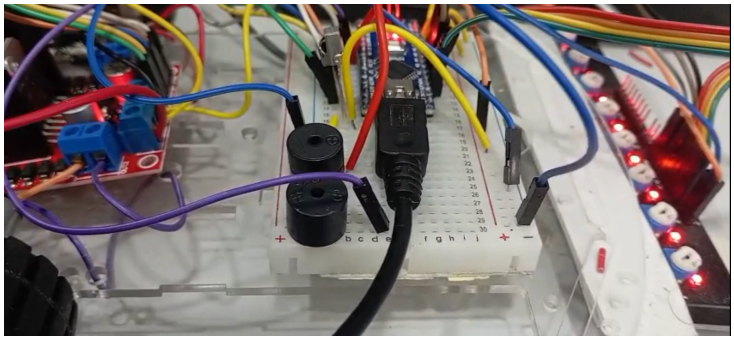

Figure 2.3: Close-up of the dual passive buzzers mounted on the breadboard, utilized for generating PWM-based auditory state feedback and critical fault alarms.

- **Critical Error Diagnostics:** If the vehicle derailed and the 360-degree recovery sweep failed to find the line within a predefined timeout period, the system entered a hard safety halt. In this state, the microcontroller generated a high-frequency, oscillating square wave to the passive buzzer, emitting a loud distress alarm to alert floor operators of a navigation failure.
- **Auditory State Feedback and Capability Demonstration:** To demonstrate the capability of the microcontroller's internal timers, the passive buzzer was additionally programmed to play complex musical melodies (such as standard holiday tunes like "Jingle Bells") upon successful boot-up or mode switching. While implemented as a creative feature, this rigorously tested the microcontroller's ability to handle non-blocking asynchronous timing functions without interrupting the mission-critical motor control loops.

Conclusion of Phase 1 and the Need for Payload Capacity: While the Phase 1 acrylic prototype successfully validated the dual-mode operational logic and the foundational analog sensor tracking, it lacked a fundamental characteristic of industrial robotics. By definition, an Automated Guided Vehicle (AGV) must not merely navigate a path; it must actively transport a payload from one node to another. The planar acrylic chassis had zero payload containment capabilities and lacked the structural rigidity required to carry localized weight. To transform the prototype from a basic line-follower into a functional AGV unit-load carrier, a complete mechanical paradigm shift was required for Phase 2.

2.7 Phase 2: Final Mechanical Design and Integration

The primary objective of Phase 2 was to develop a load-bearing chassis capable of securely housing the delicate electronic subsystems while providing a stable, isolated platform for physical payloads (such as manufactured blocks, raw materials, or tools).

2.7.1 Material Selection: The Bin-Chassis Concept

Rather than fabricating a complex sheet metal enclosure from scratch—which would introduce excessive weight and manufacturing delays—an innovative, rapid-manufacturing approach was adopted. An industrial-grade, ribbed storage bin (commonly utilized in warehouse shelving and inventory management) was selected to serve as the primary monocoque chassis.

This selection provided several immediate mechanical advantages:

- **High-Density Polyethylene (HDPE) Construction:** The bin's polymer composition provided an excellent strength-to-weight ratio, ensuring the N20 micro gear motors would not be overwhelmed by the tare weight of the vehicle itself.
- **Structural Ribbing:** As seen in standard industrial bins, the exterior walls feature vertical ribbing. This geometric design acts as a stiffener, providing high torsional rigidity and preventing the chassis from flexing when subjected to uneven payload distributions.
- **Volumetric Containment:** The deep walls of the bin naturally created a secure enclosure, preventing payloads from shifting and falling off the vehicle during sharp differential turns or sudden stops.

2.7.2 Chassis Modification and Hardware Mounting

To convert the passive storage bin into an active robotic chassis, precise subtractive manufacturing techniques (cutting and milling) were applied to the polymer shell to accommodate the drivetrain and sensory arrays.

Propulsion and Actuation Cutouts

The N20 motors required direct coupling to the wheels outside the chassis, while the sensitive wiring and L298N motor driver needed to remain securely inside. Precision rectangular cutouts were milled into the lower lateral walls

(the sides) of the bin. The motors were flush-mounted through these apertures, aligning the wheel axles directly with the center of gravity of the bin. This mid-drive configuration ensured that any payload weight placed inside the bin would press directly downward onto the drive wheels, maximizing rubber-to-surface traction and eliminating wheel slip during acceleration.

Sensor Array Aperture

For the autonomous tracking system to function, the 8-channel analog IR array required a direct, unobstructed line of sight to the floor surface, maintained at a strict millimeter-tolerance focal height. A lateral aperture was excised from the forward floor panel of the bin. The IR array was mounted flush with this cutout, allowing the sensors to scan the tape while protecting the PCB and wire harnesses from physical damage if the vehicle encountered floor debris.

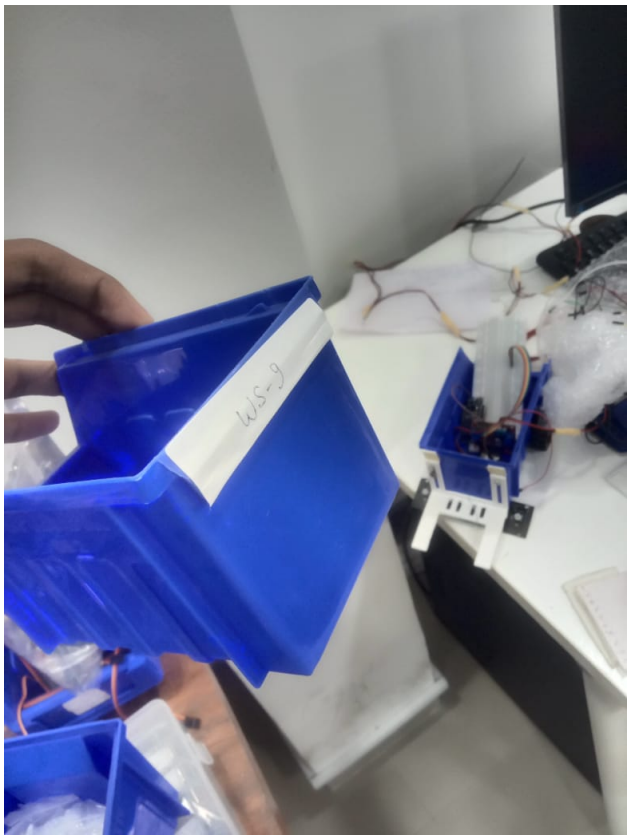

Figure 2.4: The Phase 2 industrial storage bin being modified into a monocoque chassis, illustrating the rigid sidewalls that will house the electronic subsystems and transport the physical payload.

2.7.3 Internal Decking and Payload Isolation Layer

A critical engineering challenge in unit-load AGVs is ensuring that the physical payload does not interfere with the internal avionics. In the Phase 2 design, simply dropping a payload (such as heavy blocks) into the bin would risk crushing the Arduino Nano, dislodging breadboard jumper wires, or causing electrical short circuits across the battery terminals.

To solve this, a dual-layer internal architecture was developed.

1. **The Avionics Bay (Lower Deck):** All critical electronics—including the 3-cell Lithium-Ion battery pack, the L298N motor driver, the Arduino Nano, the passive buzzers, and the internal wiring harnesses—were secured directly to the interior floor of the bin.

2. **The Payload Deck (Upper Isolation Sheet):** A custom 3D planar sheet was fabricated to act as a false floor. This sheet was securely mounted horizontally inside the bin, positioned directly above the highest electronic component.

This isolation sheet effectively split the bin into two distinct volumes. The lower volume functioned as a protected, thermally ventilated avionics bay. The upper volume functioned as the designated payload containment zone. Operators could now load blocks, tools, or irregular items directly onto the top of the 3D sheet without any risk of damaging the underlying circuitry. Furthermore, this internal deck distributed the mechanical stress of the payload evenly across the reinforced sidewalls of the bin, rather than allowing the weight to press down directly onto the thin plastic floor.

2.7.4 Conclusion of the Mechanical Phase

The integration of the industrial bin with the custom internal decking resulted in a highly robust, functional AGV capable of fulfilling its primary directive: autonomous material transport. With the mechanical architecture and hardware validation complete, the final phase of the project required developing the advanced mathematical software—specifically the Proportional-Integral-Derivative (PID) control algorithms—to allow this newly weighted vehicle to navigate complex factory paths smoothly.

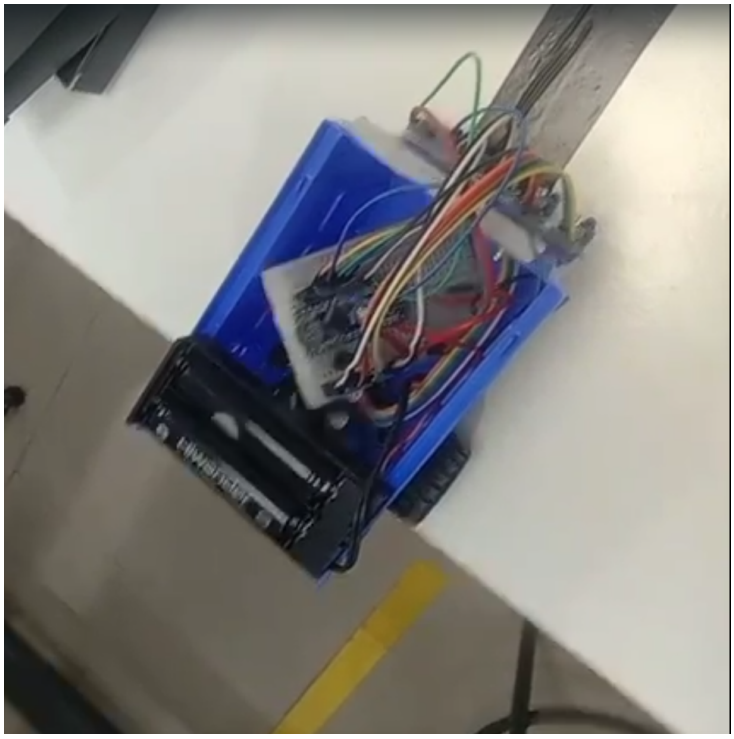

Figure 2.5: Underside view of the Phase 2 AGV chassis, revealing the external side-mounting of the N20 gear motors, the front-mounted passive caster wheel for stability, and the 8-channel analog IR sensor array positioned for floor-level tracking.

2.8 Phase 3: Electrical Architecture and Component Analysis

With the mechanical monocoque chassis established in Phase 2, the next critical step in the systems engineering process is defining the electrical architecture. The AGV operates as a tightly coupled mechatronic system, where physical navigation is entirely dependent on the precise interaction between the microcontroller, the motor drivers, and the sensory array. This section provides a rigorous theoretical analysis of the core electronic components selected for the final build.

2.8.1 Central Processing Unit: Arduino Nano (ATmega328P)

The primary computational engine of the AGV is the Arduino Nano, a compact, breadboard-friendly microcontroller board based on the 8-bit ATmega328P AVR architecture.

- **Clock Speed and Processing:** Operating at a 16 MHz clock frequency, the Nano provides sufficient processing speed to execute high-frequency control loops (such as PID calculations) without introducing mechanical latency.
- **Analog-to-Digital Conversion (ADC):** The most critical factor for selecting the Nano over the standard Arduino Uno is its pinout architecture. The ATmega328P on the Nano exposes 8 independent Analog Input pins (A0 through A7) connected to a 10-bit ADC. This allows the microcontroller to map analog voltage inputs ranging from 0V to 5V into discrete digital values between 0 and 1023. This 8-pin ADC availability is a strict hardware requirement to interface simultaneously with all eight channels of the navigation sensor array.
- **Hardware PWM:** The board features dedicated hardware Pulse Width Modulation (PWM) output pins. These are essential for sending high-frequency square waves to the motor driver to regulate the velocity of the AGV precisely.

2.8.2 Actuation Control: L298N Dual H-Bridge Motor Driver

Microcontrollers operate on low-current logic signals (typically providing a maximum of 40mA per pin at 5V). Therefore, they cannot directly drive high-

current inductive loads like DC gear motors without catastrophic thermal failure. To bridge this gap, the L298N Dual H-Bridge motor driver is utilized.

- **H-Bridge Theory:** An H-bridge is an electronic circuit consisting of four switching elements (typically transistors or MOSFETs) configured in an 'H' shape around a central motor load. By selectively opening and closing diagonal pairs of these switches, the L298N can reverse the polarity of the voltage applied to the motors, enabling the AGV to drive both forward and backward.
- **Velocity Control via PWM:** The L298N features Enable pins (ENA and ENB) for its two motor channels. By feeding a PWM signal from the Arduino into these Enable pins, the driver rapidly switches the motor power on and off. The resulting duty cycle (the ratio of 'ON' time to 'OFF' time) dictates the average voltage delivered to the motors, providing granular control over the AGV's rotational and linear speed.

2.8.3 Navigation Sensory Array: 8-Channel Analog IR

The "eyes" of the AGV consist of a specialized 8-channel Infrared (IR) sensor array mounted to the lower front chassis. Each channel on the array consists of an emitter-detector pair:

- **Infrared Emitter:** An LED that continuously projects a beam of near-infrared light downward toward the facility floor.
- **Phototransistor (Detector):** A semiconductor device that measures the intensity of the IR light reflected back from the floor.
- **Analog Voltage Gradient:** The floor surface dictates the reflection. The bright white floor highly reflects the IR light, causing the phototransistor to output a specific voltage. Conversely, the matte black tracking tape absorbs the IR light, resulting in a distinctly different voltage output. Because these are *analog* sensors, they do not simply snap between 1 and 0. If a sensor is positioned exactly on the edge of the tape, it reads a partial reflection, outputting an intermediate voltage. This analog gradient allows the software to calculate the exact millimeter position of the tape beneath the array, which is impossible with basic digital sensors.

2.8.4 Power Distribution: Lithium-Ion Battery Matrix

Industrial mobility requires a high power-density energy source capable of sustaining high discharge rates. The AGV is powered by a custom matrix of three 18650 Lithium-Ion cells wired in series (3S configuration).

- **Voltage Characteristics:** A 3S Li-ion pack provides a nominal voltage of 11.1V, reaching up to 12.6V when fully saturated.
- **Dual-Rail Distribution:** This 11.1V raw power is routed directly to the L298N module to drive the high-current N20 gear motors. Simultaneously, the 11.1V is tapped and routed into the Arduino Nano's `VIN` pin. The Nano's onboard linear voltage regulator safely steps this down to a highly stable 5V logic-level supply, which is then used to power the microcontroller chip, the IR sensor array, and the passive buzzer diagnostics.

2.9 Phase 4: Software Implementation and Advanced Control Logic

The physical construction of the Automated Guided Vehicle (AGV) provides the mechanical framework for mobility, but the autonomous intelligence of the system resides entirely within its firmware. The software was authored in C++, utilizing the Arduino hardware abstraction layer. This phase requires a rigorous mathematical understanding of control systems—specifically the Proportional-Integral-Derivative (PID) algorithm—followed by an exhaustive, line-by-line analysis of its discrete-time implementation on the highly constrained 8-bit ATmega328P microcontroller architecture.

2.9.1 Embedded Systems Constraints and Microcontroller Architecture

Developing firmware for an industrial robotic system differs vastly from writing software for a modern desktop computer. The Arduino Nano is powered by the ATmega328P, an 8-bit AVR RISC-based microcontroller. It operates at a clock frequency of 16 MHz and contains a severely limited memory architecture: 32 Kilobytes of Flash memory (for storing the compiled program) and only 2 Kilobytes of Static Random-Access Memory (SRAM) for volatile runtime data.

Because SRAM is strictly limited, dynamic memory allocation (such as using the `String` class or vectors) is actively avoided in the codebase to prevent heap fragmentation and stack overflow, which would cause a catastrophic robotic failure mid-transit. Therefore, the firmware relies on statically allocated, globally defined arrays and hardware-level constants.

2.9.2 Firmware Dissection: Memory Allocation and Hardware Mapping

The codebase begins by establishing the rigid interface between the physical wiring and the software definitions. These definitions tell the compiler exactly which physical pins on the microcontroller correspond to specific peripherals.

```
// Motor pins: [0]Left PWM, [1]Right PWM, [2,3]Left Dir, [4,5]Right Dir
const int motor_pins[6] = {9, 10, 8, 7, 6, 5};

// IR sensors (Arduino Nano)
const int sensor_pins[8] = {A0, A1, A2, A3, A4, A5, A6, A7};
const int buzz_pin = 2;
```

The `const` Keyword and Array Management

In C++, an array is a data structure consisting of a collection of elements identified by array indices. The `motor_pins` array holds 6 elements, indexed from 0 to 5. The variables are declared as `int` (integers), which consume 2 bytes (16 bits) of memory each.

Crucially, these arrays are prefixed with the `const` keyword. This informs the `avr-gcc` compiler that these values are read-only and will never mutate during runtime. As an optimization, the compiler maps these values directly into the 32 KB Flash memory, successfully preserving precious SRAM for dynamic kinematic calculations later in the program.

- **Motor Mapping:** Indices `[0]` and `[1]` map to digital pins 9 and 10. These specific pins are physically tied to Timer1 on the ATmega328P, allowing for hardware-based Pulse Width Modulation (PWM) generation to control motor velocity. Indices `[2]` through `[5]` map to standard GPIO pins for directional logic (H-Bridge switching).
- **Sensor Mapping:** The `sensor_pins` array maps directly to the multiplexed Analog-to-Digital Converter (ADC) pins (`A0-A7`).

2.9.3 Sensor Calibration and ADC Physics

Before navigating, the AGV must be mathematically calibrated to its environment. Infrared (IR) light reflects differently depending on the albedo of the floor surface.

```
// ---- CALIBRATION ----
int white_value = 200;
int black_value[8] = {800,800,800,800,800,800,800,800};
```

The microcontroller cannot read "light" or "dark"; it can only read voltage. The IR phototransistors act as variable resistors, altering the voltage on the analog pins based on light intensity. The 10-bit ADC translates this continuous $0V$ to $5.0V$ range into discrete integers from 0 to 1023.

$$\text{ADC\_Value} = \left(\frac{V_{in}}{V_{ref}} \right) \times 1023$$

The `white_value` is empirically set to 200, representing the baseline voltage step when the sensor is over the highly reflective white floor. The `black_value` is defined as an array rather than a single integer. Because mass-produced IR LEDs often exhibit minor manufacturing variances in luminosity, assigning a specific maximum absorption value (e.g., 800) to each individual sensor allows for modular, high-precision calibration.

2.9.4 Theoretical Foundation of PID Kinematics

To achieve industrial-grade tracking, the AGV utilizes a Proportional-Integral-Derivative (PID) control algorithm. Relying on simple binary logic ("if line is left, turn left") results in unstable, aggressive oscillations known as "hunting," which can destabilize heavy payloads.

A continuous PID controller calculates an error value $e(t)$ as the difference between a desired setpoint and a measured process variable. It then applies a correction based on three distinct mathematical terms. The continuous-time definition of the control variable $u(t)$ is:

$$u(t) = K_p e(t) + K_i \int_0^t e(\tau)d\tau + K_d \frac{de(t)}{dt}$$

```
// ---- PID TUNING ----
int base_speed = 180;
float kp = 25.0;
float ki = 0.0;
float kd = 15.0;
```

These variables define the aggressiveness of the control loop:

- **Proportional Gain ($K_p = 25.0$):** Dictates the immediate reaction to the current positional error. A high K_p value forces the AGV to turn sharply when the line is detected near the edge of the array.
- **Integral Gain ($K_i = 0.0$):** Integrates past errors over time to eliminate steady-state bias (e.g., if one motor gearbox has slightly higher friction). In highly dynamic, high-speed line following, accumulating integral error can cause a catastrophic failure known as "integral windup," where the robot overcompensates for an error that no longer exists. Thus, K_i is empirically set to zero.
- **Derivative Gain ($K_d = 15.0$):** Estimates the future trend of the error based on its current rate of change. It acts as a critical dampening force. As the proportional term aggressively steers the AGV back toward the center line, the derivative term actively counteracts the momentum, preventing the vehicle from overshooting the center point.

These constants are declared as `float` (32-bit floating-point numbers). While the ATmega328P lacks a hardware Floating Point Unit (FPU), making float math computationally expensive in software, the high-precision decimals are strictly necessary to prevent integer truncation during the complex calculus operations.

2.9.5 State Buffers and Positional Weights

```
// ---- STATE ----
int sensor_values[8];
float normalized[8];
int weight[8] = {-7,-5,-3,-1,1,3,5,7};

float error = 0, last_error = 0, integral = 0;
float last_side = 0;
```

The `weight` array provides the geometric mapping of the sensors relative to the physical center of the chassis. The outermost left sensor is assigned a weight of -7, while the outermost right is assigned $+7$. The state variables (`error`, `last_error`, `integral`) are global buffers initialized to 0. They act as the system's memory across multiple loop iterations, which is a mathematical prerequisite for calculating derivatives (which require a previous state) and integrals (which require an accumulated sum).

2.9.6 System Initialization: The `setup()` Routine

The `setup()` function executes exactly once upon power-up or hardware reset. Its primary role is to configure the data direction registers within the microcontroller.

```
void setup() {
  Serial.begin(115200);
  pinMode(buzz_pin, OUTPUT);

  for (int i = 0; i < 6; i++) pinMode(motor_pins[i], OUTPUT);
  for (int i = 0; i < 8; i++) pinMode(sensor_pins[i], INPUT);

  beep(100); beep(100);
  delay(1000);
}
```

- `Serial.begin(115200)`: Initializes the Universal Asynchronous Receiver-Transmitter (UART) hardware block at a high baud rate of 115,200 bps. This enables rapid telemetry streaming back to the host computer without bottlenecking the main control loop.
- **Iterative Register Configuration:** Rather than writing 14 individual `pinMode()` statements, `for` loops iterate through the `motor_pins`

and `sensor_pins` arrays. `OUTPUT` mode configures the pin to supply current (source/sink), while `INPUT` mode configures the pin into a high-impedance state to safely read external voltages without drawing current.

- **Acoustic Confirmation:** The custom `beep()` function is called to verify the logic level integrity of the buzzer circuit, followed by a blocking `delay(1000)` which pauses the processor for 1000 milliseconds. This safety buffer allows the human operator to power on the robot and remove their hands from the chassis before the motors engage.

2.9.7 The Main Control Loop: High-Frequency Execution

The `loop()` function is the core of the firmware. It executes continuously at hundreds of Hertz. The first critical phase is Environmental Acquisition and Normalization.

```
void loop() {
  float sum_norm = 0;
  float sum_norm_weight = 0;

  // 1. READ SENSORS
  for (int i = 0; i < 8; i++) {
    sensor_values[i] = analogRead(sensor_pins[i]);
    int val = constrain(sensor_values[i], white_value, black_value[i]);
    normalized[i] = (float)(val - white_value) / (black_value[i] - white_value);

    sum_norm += normalized[i];
    sum_norm_weight += normalized[i] * weight[i];
  }
```

Raw ADC values are highly susceptible to noise from ambient factory lighting or shadows. The firmware implements a robust data-cleaning pipeline:

1. **Acquisition:** `analogRead()` samples the voltage.
2. **Clamping:** The `constrain()` function strictly bounds the raw integer between the calibrated `white_value` and the specific sensor's `black_value`, rejecting anomalous noise spikes.

3. **Normalization:** The clamped integer is translated into a floating-point percentage. The C++ typecast `(float)` forces the compiler to execute floating-point division.

$$N_i = \frac{V_{current} - V_{white}}{V_{black} - V_{white}}$$

This yields a N_i value strictly between 0.0 (pure white) and 1.0 (pure black).

4. **Accumulation:** The algorithm calculates two running totals: `sum_norm` (the total mass of the line detected) and `sum_norm_weight` (the physical location of that mass multiplied by its weight).

2.9.8 Center of Mass Calculation and Fault Tolerance

```
float position;

// 2. LINE DETECTION
if (sum_norm > 0.1) {
  position = sum_norm_weight / sum_norm;

  if (position > 2) last_side = 1;
  else if (position < -2) last_side = -1;

  digitalWrite(buzz_pin, LOW);
} else {
  // Line lost
  digitalWrite(buzz_pin, HIGH);
  if (last_side < 0)
    setMotorSpeeds(-120, 120);
  else
    setMotorSpeeds(120, -120);
  return;
}
```

A standard digital sensor array can only confirm if the line is under a specific sensor (e.g., position 1, 2, or 3). Because the AGV normalizes analog data, it can utilize a "Center of Mass" weighted average formula:

$$\text{Position} = \frac{\sum_{i=0}^{7}(N_i \cdot W_i)}{\sum_{i=0}^{7} N_i}$$

If the tape is halfway between sensor index 3 (weight -1) and index 4 (weight 1), the position will precisely calculate as 0.0. This sub-millimeter tracking yields a continuous, highly precise floating-point coordinate rather than jagged integers, allowing for incredibly smooth motor actuation.

The Fault Recovery Protocol: If `sum_norm` drops below 0.1, the algorithm deduces that the vehicle has completely derailed. It executes the `else` block, activating the distress buzzer. Utilizing the `last_side` memory variable, it commands a zero-radius pivot turn (`-120, 120`) toward the side the line was last seen, rotating continuously until the line is reacquired. The `return` statement immediately terminates the current loop iteration, preventing the PID mathematics from operating on zero-value data.

2.9.9 Discrete-Time PID Implementation

If the line is successfully tracked, the geometric `position` is fed into the discrete-time PID engine.

```
// 3. PID
error = position;
integral = constrain(integral + error, -50, 50);
float derivative = error - last_error;
float correction = kp*error + ki*integral + kd*derivative;
last_error = error;
```

Because the ideal setpoint is the dead-center of the vehicle (0.0), the current `position` directly equals the `error`.

- **Discrete Integral:** The continuous integral $\int e(\tau)d\tau$ is approximated by Riemann sum accumulation: `integral + error`. The `constrain()` function acts as an aggressive anti-windup clamp, preventing the memory buffer from overflowing past ± 50.
- **Discrete Derivative:** The continuous derivative $\frac{de(t)}{dt}$ is approximated by subtracting the previous loop's error from the current error. Assuming a relatively stable loop execution time, this yields the rate of change of the error.
- **Output Correction:** The individual terms are multiplied by their respective tuned gains (K_p, K_i, K_d) and summed. This yields a single, abstract `correction` variable representing the magnitude and direction of the required steering force. The current `error` is then saved into `last_error` to be referenced in the next CPU cycle.

2.9.10 Differential Drive Kinematics and Dynamic Braking

The abstract `correction` variable must be translated into raw PWM values $(0 - 255)$ to drive the physical H-Bridge.

```
// 4. MOTOR SPEED
int dynamic_base = base_speed - abs(correction * 0.5);
dynamic_base = max(dynamic_base, 40);

int left_speed  = dynamic_base + correction;
int right_speed = dynamic_base - correction;

left_speed  = constrain(left_speed, -180, 255);
right_speed = constrain(right_speed, -180, 255);

setMotorSpeeds(left_speed, right_speed);
```

A critical challenge in industrial robotics is high-speed cornering. If the AGV enters a sharp curve at full `base_speed`, inertia will cause it to understeer and derail, regardless of the steering correction. To mitigate this, the code implements **Dynamic Braking**.

The `dynamic_base` speed is automatically reduced proportionally to the severity of the turn. The `abs()` (absolute value) function removes the directional sign from the correction, ensuring the base speed drops whether the vehicle turns left or right. The `max()` function guarantees the base speed never drops below 40 PWM, which is the mechanical stall-torque threshold of the N20 motors.

Differential steering kinematics are then applied: the correction is added to the left wheel and subtracted from the right wheel. Finally, `constrain()` bounds the calculated speeds between -180 (maximum safe reverse PWM for tight pivoting) and 255 (the absolute 8-bit hardware maximum).

2.9.11 Motor Actuation Abstraction Layer

The bottom of the source file houses custom subroutine functions to keep the main kinematic loop readable and modular.

```
void setMotorSpeeds(int left, int right) {
  analogWrite(motor_pins[0], abs(left));
  digitalWrite(motor_pins[2], left >= 0 ? LOW : HIGH);
  digitalWrite(motor_pins[3], left >= 0 ? HIGH : LOW);
```

```
  analogWrite(motor_pins[1], abs(right));
  digitalWrite(motor_pins[4], right >= 0 ? LOW : HIGH);
  digitalWrite(motor_pins[5], right >= 0 ? HIGH : LOW);
}
```

The `setMotorSpeeds` function abstracts the complex logical routing required by the L298N H-Bridge. Hardware PWM registers cannot interpret negative numbers. Therefore, the function passes the absolute value (`abs(left)`) to the `analogWrite()` command to dictate raw speed.

Simultaneously, it utilizes a C++ ternary operator (`condition ? true : false`) to evaluate the sign of the requested speed. If the `left` speed is positive ($>= 0$), it sets the IN1 and IN2 directional pins to `LOW` and `HIGH`, forcing forward rotation. If the calculated PID speed drops into the negative (indicating an extremely sharp curve requiring a pivot), the ternary operator flips the logic pins to `HIGH` and `LOW`, actively reversing the inside wheel to minimize the turning radius.

2.10 Conclusion

The development of the Automated Guided Vehicle (AGV) documented in this chapter represents a comprehensive exercise in full-stack mechatronic engineering. The primary objective was not merely to construct a basic line-following robot, but to design, prototype, and program an autonomous, fault-tolerant unit-load carrier capable of operating within an industrial environment.

Through a structured, four-phase engineering approach, the project successfully transitioned from theoretical kinematics to a physical, payload-bearing reality:

- **Mechanical Evolution:** The transition from the Phase 1 acrylic planar chassis to the Phase 2 High-Density Polyethylene (HDPE) monocoque bin successfully demonstrated the fundamental requirement of an AGV: payload capacity. The integration of an internal isolation deck ensured that the physical payload remained entirely decoupled from the sensitive avionics housed below.

- **Hardware Architecture:** The selection of the ATmega328P (Arduino Nano) proved highly effective. By strategically mapping its 8-channel Analog-to-Digital Converter (ADC) to the high-resolution IR array, the system achieved the sub-millimeter environmental perception required for smooth navigation.

- **Algorithmic Sophistication:** The firmware transcended basic binary logic by implementing a continuous-feedback Proportional-Integral-Derivative (PID) control system. By converting continuous-time calculus into discrete-time approximations mapped to the microcontroller's limited SRAM, the AGV achieved industrial-grade trajectory smoothing. The inclusion of dynamic braking and differential reversing further allowed the vehicle to negotiate sharp kinematic curves without derailing under inertia.

- **Fault Tolerance and Redundancy:** Recognizing the unpredictability of physical environments, the integration of a dual-mode operational architecture (allowing instantaneous teleoperated manual override via NEC protocol decoding) and an autonomous 360-degree acoustic fault-recovery sweep ensured the system remained highly resilient to tracking failures.

Ultimately, this project successfully bridged the gap between theoretical control systems and practical, embedded C++ software development. The

resulting vehicle stands as a robust, functional prototype of modern industrial material-handling robotics.

Chapter 3

Internship Project 2: Automated Conveyor System

3.1 Phase 1: Introduction to Conveyor Systems and Material Handling

In the broader context of industrial automation, mechatronics, and supply chain logistics, material handling is rigorously divided into two primary operational categories: **Discrete Transport** and **Continuous Transport**. While the Automated Guided Vehicle (AGV) developed in the previous chapter represents the pinnacle of flexible, discrete transport — capable of navigating dynamically through complex facility environments to deliver individual payloads on demand — it fundamentally relies on a stationary, high-throughput infrastructure to supply and receive those discrete payloads at fixed interchange nodes. This foundational infrastructure is overwhelmingly dominated by the continuous transport mechanism universally known as the **Conveyor System**.

A conveyor system is a sophisticated assembly of **Mechanical Handling Equipment (MHE)** engineered to actively and continuously move bulk materials or discrete unit loads from one predefined spatial coordinate to another, at a controlled, repeatable velocity, without interruption. They are especially critical in applications involving the transportation of heavy, bulky, or high-volume materials where human manual handling would be physically impossible, economically prohibitive, or unacceptably hazardous. This renders them ubiquitous and indispensable in modern manufacturing plants, automated packaging facilities, global distribution centers, mining operations, food processing lines, airport baggage handling systems, and pharmaceutical production environments.

By utilizing **rotational mechanical actuation** to drive a continuous loop of material — the **Belt** — over a series of strategically spaced, low-friction cylindrical supports — the **Rollers** or **Idlers** — conveyors drastically reduce the kinetic energy, electrical power, and human labor required to move mass over extended physical distances. The fundamental engineering elegance of the conveyor lies in its conversion of the inefficient, energy-wasteful act of repeatedly accelerating and decelerating discrete loads into a single, sustained, steady-state mechanical motion of extremely high energetic efficiency.

The economic and societal impact of the conveyor system is immeasurable. It is not an overstatement to assert that the modern industrial world — characterized by affordable mass-produced consumer goods, globally integrated supply chains, and next-day parcel delivery — could not exist in its present form without the conveyor. Every automobile, every packaged food item, every parcelled e-commerce order, and every ton of mined mineral commodity reaches its destination through a conveyor system at some point in its journey from raw material to end consumer.

3.1.1 Fundamental Physics and Mechanical Principles

To design, select, and optimize an automated conveyor system, one must first develop a rigorous understanding of the classical mechanics that govern its operation. A conveyor is, at its most fundamental level, an applied study in the interrelated disciplines of **Tribology** (the science of friction, lubrication, and wear), **Structural Mechanics** (the science of stress, strain, and material deformation under load), and **Rotational Dynamics** (the science of torque, angular momentum, and power transmission).

Belt Tension and the Friction Drive Mechanism

The movement of the belt is achieved exclusively through **Friction Drive Transmission**. The system relies on a powered **Drive Pulley** — typically a high-inertia steel cylinder directly coupled to a high-torque electric gear-motor via a keyed shaft — and an unpowered **Tail Pulley** positioned at the opposite terminus of the conveyor frame. The continuous belt loop is threaded around both pulleys and tensioned by a **Take-Up Assembly**, which may be of the screw-adjustment type on short conveyors or the gravity-weighted counterbalance type on long, heavy-duty mining conveyors.

- **Effective Tension (T_e):** This is the net driving force that the drive pulley must transmit to the belt to overcome all resistive forces and

maintain the belt at its design velocity. It is the algebraic difference between the **Tight Side Tension** (T_1, the tension in the belt leaving the drive pulley) and the **Slack Side Tension** (T_2, the tension in the belt approaching the drive pulley): $T_e = T_1 - T_2$.

- **The Euler-Eytelwein Equation:** The fundamental relationship governing the maximum transmissible friction force between the drive pulley and the belt is described by the **Euler-Eytelwein capstan equation**:

$$\frac{T_1}{T_2} = e^{\mu\theta}$$

  Where μ is the **coefficient of friction** between the pulley lagging and the belt's bottom cover, θ is the **angle of wrap** (in radians) of the belt around the drive pulley, and e is Euler's number (approximately 2.718). This equation reveals that the ratio of tight-side to slack-side tension increases exponentially with both the coefficient of friction and the wrap angle — which is why drive pulleys are often equipped with grooved rubber lagging (to increase μ) and snub pulleys are positioned near the drive pulley (to increase θ).

- **Belt Tension Limits:** The belt must be maintained within a precise tension window. If tension falls below the **minimum tension threshold**, the drive pulley will slip against the belt, generating destructive frictional heat and causing rapid belt surface degradation. If tension exceeds the **maximum allowable tension**, determined by the tensile strength rating of the belt's carcass reinforcement, the belt risks permanent elongation, carcass delamination, or catastrophic tensile rupture.

- **Coefficient of Friction (μ):** The driving force is directly proportional to μ between the drive pulley's lagging and the bottom cover of the belt. Dry rubber-on-rubber contact yields $\mu \approx 0.35$–0.40. The presence of water, oil, or fine dust contamination at this interface can reduce μ to as low as 0.10–0.15, drastically reducing the transmissible drive force and risking belt slip — a primary reason why drive pulley housings on outdoor conveyors are equipped with weather-protective shrouds.

Power Requirements and Resistive Forces

The motor must generate sufficient **Torque** (τ) to overcome the combined resistive forces acting against belt motion under the worst-case loading condition — typically full-load startup from rest, which imposes the highest

instantaneous inertial demand on the drive system. The total **Mechanical Power** required is:

$$P = \frac{(F_f + F_g + F_i + F_b) \cdot v}{\eta}$$

Where:

- F_f = **Frictional Resistance**: The sum of rolling resistance from all idler bearings along the full conveyor length, plus the sliding resistance between the belt and any stationary components such as skirting boards at the loading zone. This is typically the dominant resistive force on long, lightly loaded horizontal conveyors.
- F_g = **Gravitational Resistance**: The component of gravitational force acting along the belt's direction of travel, equal to $m \cdot g \cdot \sin\theta$ where m is the total mass of belt and payload and θ is the angle of inclination. This force is zero on horizontal conveyors, resistive on inclined conveyors, and *assistive* on decline conveyors (where it can cause the belt to overrun the drive, requiring regenerative braking).
- F_i = **Inertial Resistance**: The force required to accelerate the belt, idlers, pulleys, and payload from rest to the design operating velocity during startup. It is governed by Newton's Second Law: $F_i = m_{total} \cdot a$, where a is the design acceleration rate.
- F_b = **Bulk Material Resistance**: The force required to continuously lift and accelerate the incoming feed material from rest to belt speed at the loading point. This is particularly significant on high-tonnage conveyors fed by large-capacity hoppers or crushers.
- v = **Belt Velocity** (m/s): The linear speed of the belt surface, directly determining the volumetric throughput capacity of the conveyor.
- η = **Mechanical Efficiency** of the complete drive train, encompassing gear reducer efficiency (≈ 0.95–0.98 per stage), coupling efficiency, and bearing losses.

Conveyor Capacity and Throughput

The **Volumetric Throughput Capacity** (Q_v) of a belt conveyor — the volume of bulk material transported per unit time — is a function of the **Cross-Sectional Area** of the material load on the belt (A) and the **Belt Velocity** (v):

$$Q_v = A \cdot v \cdot 3600 \quad (\mathrm{m}^3/\mathrm{hr})$$

The cross-sectional area A is determined by the belt width, the trough angle of the idler set, and the **Angle of Repose** of the bulk material — the maximum angle at which a loose granular material will remain stationary on an inclined surface without sliding. Materials with a high angle of repose (such as moist clay or wood chips) can be carried at a higher cross-sectional fill than materials with a low angle of repose (such as dry sand or fine coal), which tend to slump and spill over the belt edges on inclines or during sudden deceleration. The **Mass Throughput** (Q_m, in tonnes/hr) is obtained by multiplying Q_v by the **Bulk Density** (ρ_b) of the material: $Q_m = Q_v \cdot \rho_b$.

3.1.2 Historical Evolution of Continuous Transport

To fully contextualize the engineering principles behind modern sensor-driven conveyors, it is essential to trace their historical evolution across six distinct and well-defined technological eras. The conveyor belt has undergone over two centuries of iterative mechanical, material science, and digital refinement — each era shaped decisively by the dominant industrial imperatives, economic pressures, and technological capabilities of its time. Understanding this evolutionary arc is not merely of academic interest; it reveals the logical engineering necessity behind every structural feature and operational characteristic of the modern automated conveyor.

Era I: The Ancient and Pre-Industrial Origins (Antiquity to 17th Century)

The conceptual and mechanical foundations of continuous material transport predate the Industrial Revolution by several millennia, demonstrating that the fundamental human imperative to move materials efficiently is as old as civilization itself.

The earliest known continuous conveyance mechanism is the **Archimedean Screw**, a device attributed to the preeminent Greek mathematician, physicist, and engineer **Archimedes of Syracuse** circa 250 BCE. This elegant helical device, when rotated continuously about its longitudinal axis by manual or water-wheel-driven power, causes water or granular solids to be progressively elevated from a lower datum to a higher one through the advancing helical cavity formed between the screw flights and the enclosing cylindrical housing. It represents the first recorded application of **sustained rotational mechanical actuation** to achieve **continuous material displacement** — the precise physical principle that underpins every modern conveyor

system, from the humblest factory roller conveyor to the most sophisticated high-speed airport baggage sorter. The Archimedean screw was deployed at industrial scale throughout the ancient Mediterranean world for agricultural irrigation, ship bilge drainage, and the dewatering of mine workings, and its fundamental operating principle remains in active commercial use today in the form of the modern enclosed **screw conveyor** and the **screw press** used in food processing and wastewater treatment.

In ancient China, **chain-driven bucket elevators** constructed from bamboo segments and timber were documented in agricultural texts as early as 100 CE for the continuous elevation of irrigation water to terraced rice paddy systems. These systems simultaneously embodied three of the four fundamental mechanical elements of a modern conveyor: a **continuous looped carrier medium** (the chain), discrete **load-bearing carrying elements** (the buckets), and a **rotational drive mechanism** (the water wheel or animal-powered capstan). This conceptual framework — continuous loop, discrete carriers, rotational drive — remains the architectural basis of every **bucket elevator**, **trolley conveyor**, and **slat conveyor** in operation today.

Concurrently, **Egyptian construction engineering** employed highly organized arrays of lubricated wooden sliders and cylindrical **log rollers** positioned beneath stone sledges to dramatically reduce the effective **coefficient of kinetic friction** during the transportation of multi-ton limestone and granite blocks from quarry faces to pyramid construction sites. By substituting **rolling contact** for **sliding contact** at the load-bearing interface, Egyptian engineers reduced the draught force required to move a given load by a factor of approximately five to ten — precisely the same tribological principle exploited by the **idler roller** in modern belt conveyor design, and by the **roller conveyor** used universally in modern warehousing and distribution.

During the European medieval period (approximately 500–1400 CE), millwrights developed increasingly refined systems of **gravity-fed grain chutes**, **leather apron slides**, and rudimentary woven-fabric conveying troughs within the confined internal spaces of water-powered grain mills to channel grain continuously from roof-level storage lofts to the millstones below. Although these systems were entirely unpowered — relying on gravitational potential energy rather than mechanical drive — they established and codified the critical operational concept of **continuous, uninterrupted material flow**: the defining characteristic that distinguishes a conveyor system from all forms of discrete batch transport. The medieval millwright's intuitive grasp of controlled flow management is directly reflected in the design philosophy of the modern **gravity roller conveyor**, the **chute transfer**

system, and the **decline conveyor**.

The Renaissance period (approximately 1400–1600 CE) brought a profound intensification of systematic mechanical thinking in Europe. **Leonardo da Vinci** (1452–1519), in his voluminous technical notebooks, sketched numerous mechanical devices incorporating continuous chain mechanisms, rotating drum drives, and linked carrier systems that bear unmistakable conceptual resemblance to modern conveyor designs. While Leonardo's visionary inventions were not fabricated or deployed in his lifetime — the material science and precision manufacturing capabilities of Renaissance Europe being wholly inadequate to realize them — his notebooks demonstrate that the **conceptual framework** for sophisticated continuous mechanical material handling was taking systematic shape among the most advanced engineering minds of the era, laying an intellectual foundation upon which later inventors would build.

Era II: The Agrarian and Mining Origins (Late 18th to 19th Century)

The earliest recorded **mechanically powered** continuous transport systems date to the late 18th century, driven by the acute operational demands of two dominant industries: **commercial grain handling** — the need to load bulk grain into granaries and naval supply vessels rapidly and at volume — and **deep-vein coal mining** — the urgent need to transport extracted coal from underground workfaces to surface stockpiles continuously and safely. These twin industrial imperatives established the two primary conveyor application domains — **unit load handling** and **bulk material transport** — that remain the organizing framework of conveyor engineering to this day.

The primitive grain-loading conveyors of the late 18th century consisted of raw, untreated leather or woven canvas belts stretched tautly over flat wooden slider beds and actuated by manual hand-cranks or localized water wheels. They required constant manual lubrication to mitigate the severe **sliding friction** between the belt underside and the stationary wooden bed, and their operational spans were severely limited by the low tensile strength of the belt materials and the inadequate drive forces achievable with manual or simple water-wheel actuation. Despite these severe limitations, they demonstrated unambiguously the fundamental economic viability of continuous belt conveying for granular bulk material handling — a proof of concept that would catalyze a century of progressive engineering refinement.

A pivotal and transformative engineering contribution during this foundational period was made by the American inventor and engineer **Oliver Evans** (1755–1819), who in 1795 designed, constructed, and operated a fully

integrated, largely automated flour mill at Red Clay Creek, Delaware. Evans' mill was a revolutionary system that combined **bucket elevators** for vertical grain elevation, **screw conveyors** (descended directly from the Archimedean principle) for horizontal grain distribution between processing stages, and **continuous leather belt conveyors** for inter-floor product transfer — all driven by a single water wheel through a network of mechanical power transmission shafting. Raw grain entered the mill at one end, and finished, packaged flour emerged at the other with minimal human intervention, in a continuous, uninterrupted mechanical flow. Evans' mill is widely recognized by historians of technology as arguably the **world's first fully automated, integrated production system** — a conceptual precursor to the modern **automated production line** that predates Ford's assembly line by over a century. Evans patented his mill design and described it exhaustively in his influential 1795 treatise *The Young Mill-Wright and Miller's Guide*, which served as the definitive technical reference for American mill engineering for decades.

The **first major industrial paradigm shift in heavy-duty continuous conveying** occurred in 1892, when the American mechanical engineer **Thomas Robins** developed, patented, and commercially deployed a purpose-designed heavy-duty conveyor system specifically engineered to transport the highly abrasive, heavy, and irregularly sized materials — coal, crushed rock, and metallic ores — that the rapidly expanding mining industry needed to move in enormous quantities from excavation faces to processing plants or transport infrastructure. Robins' revolutionary design introduced the concept of **Troughed Idler Rollers** — sets of three free-spinning, cylindrical steel tubes arranged in a symmetrical trough formation beneath the loaded carrying strand of the belt — which simultaneously supported the weight of the loaded belt across its full span, formed the belt into a trough-shaped cross-section that dramatically increased its volumetric carrying capacity relative to a flat belt of the same width, and reduced the **effective surface contact friction** between the belt underside and its support structure by replacing continuous sliding contact against a flat wooden bed with intermittent **rolling contact** at widely spaced bearing points. This three-fold functional achievement — load support, capacity increase, and friction reduction — allowed the Robins system to span vastly greater horizontal distances without the belt snapping under immense tensile stress. The **Robins troughed idler belt conveyor** is the direct mechanical and conceptual ancestor of virtually every modern heavy industrial belt conveyor in worldwide operation today, and the troughed idler set remains the universal standard for bulk material belt conveyor design.

In parallel developments on the other side of the Atlantic, the British

engineer **Richard Sutcliffe** of Yorkshire patented and successfully commercialized rubber-fabric belt conveyors specifically designed for **underground coal mine haulage** during the 1860s and 1870s. The operational environment of an underground coal mine presented an extraordinarily hostile proving ground for conveyor technology: extreme space constraints in low-height mine roadways, heavy abrasive coal loading, the constant presence of water and coal dust, and the ever-present risk of fire and explosion imposed by **firedamp** (methane) and coal dust in suspension. Sutcliffe's robust rubber-fabric belts, designed to withstand these conditions while operating reliably over the extended periods demanded by continuous production mining, replaced the dangerous and labor-intensive practice of manual hauling and pony-drawn tub haulage within mine galleries. By demonstrating that continuous belt conveying was economically viable, practically reliable, and operationally superior to all alternative haulage methods in even this most demanding of industrial environments, Sutcliffe's work established **mine haulage** as the primary high-volume proving ground for belt conveyor technology — a role it has retained to the present day, with modern underground mines deploying belt conveyor systems of extraordinary capacity and sophistication.

The development of **steam-powered bucket grain elevators** in the United States during the 1840s completed the foundational infrastructure of the 19th-century grain trade. The world's first steam-powered grain elevator, constructed by **Joseph Dart** and engineered by **Robert Dunbar** in **Buffalo, New York** in 1842, used a continuous loop of canvas buckets driven by a steam engine to elevate bulk grain from the holds of Great Lakes cargo vessels and discharge it into storage bins at rates previously unimaginable with manual handling methods. The Buffalo elevator could unload a fully laden lake vessel in hours rather than the days required by gang labor. This transformative productivity gain effectively resolved a severe logistical bottleneck that had been constraining the growth of the American grain trade, and the steam-powered bucket elevator rapidly proliferated along the entire Great Lakes and Mississippi River grain transportation network, enabling the agricultural productivity of the expanding Midwest to be efficiently integrated with the global commodity markets of the eastern seaboard and Europe.

Era III: The Mass Production Paradigm (Early 20th Century)

The most profound **cultural, economic, and social** transformation in the entire history of the conveyor system occurred on the afternoon of **October 7, 1913**, when **Henry Ford** and his production engineers — princi-

pally **Charles Sorensen** and **Clarence Avery** — implemented the world's first **continuously moving automobile assembly line** at Ford's Highland Park manufacturing plant in Detroit, Michigan. The fundamental operational insight behind this innovation was deceptively simple yet profoundly revolutionary: rather than having workers carry components to a stationary vehicle chassis positioned on the factory floor — an arrangement that wasted the majority of each worker's time in walking, searching, and positioning — the conveyor system would bring the chassis continuously and at a precisely controlled velocity past the workers, each of whom was permanently stationed at a fixed point on the line and trained to perform a single, highly specialized, repetitive assembly task with maximum speed and efficiency.

This application of the conveyor to manufacturing process management did not merely transport material from one location to another; it fundamentally and permanently **restructured the human relationship to industrial labor** and the **temporal architecture of manufacturing**. The conveyor became the **mechanical metronome** of the factory — an impartial, unceasing mechanical arbiter of production pace that enforced a uniform cadence upon every human worker and every mechanical process within the facility. A worker could not fall behind the line without impeding the entire production flow; the conveyor made individual pace variation structurally impossible and transformed the factory into a single, synchronised, continuous-flow production machine.

The quantitative results were historic and immediate. Ford reduced the time required to completely assemble a Model T automobile from over **12 hours and 28 minutes** (under the stationary chassis assembly method) to **93 minutes** — a productivity improvement of approximately **700%** achieved through a purely organizational and mechanical innovation, without any fundamental change to the components being assembled or the tools used to assemble them. This dramatic reduction in assembly labor cost per vehicle allowed Ford to continuously reduce the retail price of the Model T from **$850 in 1908** to **$290 by 1924**, placing private automobile ownership for the first time within the economic reach of the ordinary American working-class family and creating an entirely new mass consumer market that transformed American society. The Ford assembly line model was rapidly and comprehensively adopted by manufacturers of consumer goods, domestic appliances, military armaments, aircraft, radio sets, and industrial equipment across the entire industrialized world within a decade of its introduction, making it arguably the single most imitated and economically influential manufacturing innovation of the 20th century.

The proliferation of mass production assembly lines across global industry also drove the parallel development and widespread adoption of **Over-**

head Trolley Conveyor Systems — in which product carriers, fixtures, or hanging hooks are suspended from **motorized drive chains** running along elevated **I-beam tracks** mounted to the facility ceiling or structural steelwork. Overhead conveyors provided three critical operational advantages that ground-level belt conveyors could not: they completely **liberated the factory floor** from material handling infrastructure, freeing it for unobstructed worker movement, machine placement, and AGV navigation; they enabled products to be continuously transported **between different floor levels** within a multi-story facility without the interruption and bottleneck risk of manual transfer; and they allowed products to be conveyed **directly through continuous-process treatment stations** — such as **chemical degreasing baths**, **electroplating tanks**, **phosphating dip tanks**, **paint spray booths**, and **curing ovens** — with the product remaining suspended on its carrier throughout the treatment process, eliminating repeated loading and unloading operations and ensuring uniform treatment exposure time.

Era IV: The Synthetic Materials Revolution (Post-WWII, 1945–1970)

Following the conclusion of World War II, the materials engineering science underlying conveyor belt manufacturing evolved with a rapidity and depth of innovation that fundamentally expanded the operational scope and environmental range of conveyor deployment. The wartime synthetic materials research programs of the United States and Germany — which had produced advances in **synthetic rubber compounding**, **polymer chemistry**, **nylon and polyester fiber production**, and **high-strength steel wire drawing** — were rapidly translated into commercial conveyor belt products of dramatically superior performance characteristics.

Pre-war natural rubber and woven cotton canvas conveyor belts exhibited severe and well-documented vulnerabilities: **thermal degradation** and accelerated aging at operating temperatures above approximately 70°C; **chemical corrosion and swelling** upon contact with hydrocarbon oils, aromatic solvents, and strong acids or alkalis; **hygroscopic moisture absorption** in humid environments causing progressive weakening and rotting of the cotton canvas carcass; and **structural delamination and tensile rupture** under the heavy impact loading imposed by large-lump rock and ore falling from considerable heights onto the belt at loading points. These limitations confined pre-war conveyors to relatively benign operational environments and moderate load intensities.

The post-war introduction of **Synthetic Polymer Belt Covers** — principally **vulcanized styrene-butadiene rubber (SBR)**, **neoprene**

(polychloroprene), **nitrile rubber (NBR)** for oil-resistant applications, **EPDM** for high-temperature applications, and **thermoplastic polyurethane (TPU)** for high-wear, food-contact, and pharmaceutical applications — combined with **Synthetic Fiber Carcass Construction** using high-tenacity **nylon (polyamide)** and **polyester (PET) woven fabrics**, produced belt constructions with dramatically superior resistance profiles across all failure modes simultaneously. Nylon-polyester carcass belts offered higher tensile strength, lower elongation under load, superior impact resistance, and essentially zero moisture absorption compared to their cotton canvas predecessors, while synthetic rubber covers provided reliable performance across temperature ranges from −40°C to +200°C and resistance to virtually all commercially significant chemical environments.

The most strategically significant materials innovation of this era, however, was the commercial development and industrial deployment of **Steel-Cord Reinforced Belt Construction**, in which the traditional multi-ply woven fabric carcass is entirely replaced by a parallel array of **high-tensile stranded steel wire cables** (typically 2.5–10 mm in diameter) embedded longitudinally within the rubber belt body at regular lateral spacings. Steel-cord belts offered **tensile strength ratings** of up to 10,000 N/mm of belt width — compared to 1,000–3,000 N/mm achievable with the strongest fabric-ply constructions — combined with **extremely low elastic elongation** under load (typically less than 0.25% at rated working tension, compared to 1.5–3.0% for fabric belts), allowing the belt to maintain consistent sag geometry between idlers without the constant re-tensioning that plagued long fabric-ply conveyors as their carcasses crept under sustained load. These properties enabled **single-flight belt conveyor systems** of previously inconceivable length to be economically constructed and reliably operated in major mining and bulk handling projects. The world's longest single belt conveyor flight — the **OCP phosphate mine conveyor system** in the Western Sahara, Morocco — spans approximately **98 kilometers** and transports phosphate rock from the inland Bou Craa mine to the coastal export terminal at El Aaiun, representing the ultimate product of this materials engineering lineage.

Era V: The Electronic Control and Automation Era (1969–2000)

The introduction of the **Programmable Logic Controller (PLC)** by **Dick Morley** and the **Modicon Corporation** in 1969 — developed originally to replace the enormous and inflexible banks of electromechanical relay logic panels used to control the highly complex automated transfer lines of the American automotive industry — marked the precise historical inflection

point at which the conveyor system began its transformation from a passively mechanical transport device into an **actively intelligent, programmable process control system**.

Prior to the PLC, all conveyor control logic was implemented entirely in **hardwired electromechanical relay circuits**. Each conditional logical function — "if sensor A is activated AND sensor B is not activated AND timer C has elapsed, THEN energize motor contactor D" — required one or more physical relay devices, wired permanently into a control panel that could occupy an entire wall of a factory's electrical room. These systems were not merely large and expensive; they were fundamentally **inflexible**. Modifying the control logic of a relay-controlled conveyor system required physical rewiring of the relay panel — a time-consuming, labor-intensive, and error-prone process that could take weeks and required electrical engineering expertise. In an industrial environment where product ranges, production schedules, and routing requirements changed frequently, relay-controlled conveyors imposed severe operational rigidity.

The PLC resolved all of these limitations simultaneously by replacing hardwired relay logic with **software-defined ladder logic programs** stored in solid-state electronic memory and executed cyclically by a dedicated microprocessor. The entire control behavior of a conveyor system could now be defined, modified, debugged, documented, and archived as a software program — reprogrammable in hours rather than weeks, copyable and transferable between controllers, and executable with perfectly consistent timing and logic evaluation on every program scan cycle. This programmability unlocked a generation of sophisticated **dynamic conveyor capabilities** that were structurally impossible with relay logic: **automated product counting and throughput rate calculation**; **conditional divert gate actuation** based on barcode-scanned destination codes or weight-classified product categories; **zone-by-zone speed modulation** to prevent downstream accumulation bottlenecks; **automatic fault detection** and **alarm annunciation** upon sensor failure, belt mis-tracking, or motor overload; and **timed sequential interlocking** between multiple interconnected conveyor lines to ensure coordinated startup and shutdown sequences that prevent material surges and spillage.

The commercial maturation of **Industrial Barcode Scanning Technology** during the 1970s and 1980s provided the identification and sensing infrastructure that made **automated, high-speed conveyor sortation** economically viable and operationally reliable at industrial scale. By integrating **fixed-mount helium-neon laser barcode readers** positioned above conveyor lines at strategic scanning points, distribution centers, parcel processing facilities, and postal automated letter and flat-mail sorting

plants could automatically identify every individual item moving along the conveyor line, interrogate a **warehouse management system (WMS)** or **sortation control system** database via real-time network communication to determine the correct outbound destination, and actuate the appropriate **divert mechanism** — a **pop-up wheel diverter**, a **tilt-tray carrier**, a **crossbelt transfer**, or a **paddle arm pusher** — at precisely the correct moment to route the item to the designated outbound lane, shipping dock, or dispatch chute. All of this was achieved without any human sorting intervention, at throughput rates of hundreds to thousands of items per hour per sortation line.

This automated sortation capability did not merely improve the efficiency of existing operations; it **fundamentally transformed the economic model** of parcel logistics, postal services, and retail distribution. Companies such as **FedEx**, **United Parcel Service (UPS)**, and national postal services throughout the world invested billions of dollars in high-speed automated conveyor sortation infrastructure during the 1980s and 1990s, enabling the next-day and time-definite parcel delivery services that have become the operational backbone of modern business logistics and, subsequently, global e-commerce.

The concurrent development and widespread industrial adoption of **Variable Frequency Drive (VFD) technology** — electronic power converters that allow AC induction motors to be operated at continuously variable speeds by varying the frequency and voltage of the electrical supply — provided conveyor system designers with a degree of operational speed flexibility that had never previously been achievable with direct-on-line motor starting. VFD-controlled conveyors could **accelerate smoothly and gradually** from rest to full operating speed using a controlled ramp function, eliminating the severe mechanical shock loads and belt tension spikes imposed by direct motor starting that had historically caused premature belt, coupling, and gearbox failures on heavy-duty conveyors. VFDs also enabled **dynamic speed adjustment** during operation in response to real-time throughput demand signals from upstream or downstream processes, and facilitated **regenerative braking** on decline conveyors — recovering the gravitational potential energy of the descending load as electrical energy returned to the supply grid, rather than dissipating it wastefully as heat in mechanical brake drums.

Era VI: Cyber-Physical Integration and Industry 4.0 (2000–Present)

The final and most consequential evolutionary transformation of the conveyor system — and the era that provides the direct intellectual and engineering context for this internship project — is the comprehensive integration of **dig-**

ital intelligence, **networked embedded computing**, **advanced sensing systems**, **machine learning algorithms**, and **autonomous robotic collaboration** into what were previously purely mechanical material transport devices, creating what engineers and industrial technologists describe as the **Cyber-Physical Conveyor System**.

The transition from PLC-controlled to **IIoT-integrated** (Industrial Internet of Things) conveyor systems brought about by advances in **low-cost MEMS sensor technology**, **industrial wireless communication protocols** (such as WirelessHART, ISA100, and 5G industrial cellular), and **cloud computing platforms** enabled real-time monitoring of conveyor mechanical health at a granularity and comprehensiveness never previously achievable. Modern conveyor systems are equipped with **tri-axial vibration sensors** mounted on every idler bearing housing along the conveyor length, **infrared thermal imaging cameras** that continuously scan the belt surface and idler frames for hotspots indicative of seized bearings or belt cover vulcanization degradation, **laser belt tracking sensors** that monitor belt lateral displacement in real-time and automatically adjust take-up tension to correct mis-tracking before it causes edge damage, and **ultrasonic thickness gauges** that measure the remaining rubber cover thickness on the belt surface to predict the remaining service life before carcass exposure. All of this condition monitoring data is transmitted continuously to **cloud-hosted predictive maintenance analytics platforms** that apply machine learning algorithms to detect anomalous vibration signatures, thermal patterns, or thickness trends that indicate developing component faults — typically days or weeks before the fault would manifest as a catastrophic failure — and automatically generate **work orders** in the facility's **Computerized Maintenance Management System (CMMS)** for the preventive replacement of the identified component at the next scheduled maintenance window.

The explosive growth of **e-commerce** — catalyzed by Amazon (founded 1994) and accelerating exponentially through the 2000s, 2010s, and beyond — imposed fundamentally new and extraordinarily demanding performance requirements on conveyor and sortation systems that drove the most rapid period of technological innovation in conveyor history since Ford's assembly line. E-commerce fulfillment is operationally antithetical to conventional retail distribution: whereas retail distribution ships **full pallets** of identical products to a small number of store locations on predictable, schedule-driven cycles, e-commerce fulfillment requires the **individual picking, packing, and shipping** of millions of unique, single-item orders daily, each to a different address, with consumer expectations of same-day or next-day delivery that leave no margin for operational inefficiency. Meeting this challenge has required conveyor systems of unprecedented speed, flexibility, accuracy, and

throughput density, tightly integrated with advanced robotic picking, vision inspection, and autonomous mobile transport systems.

The modern **hyperscale e-commerce fulfillment center** — exemplified by Amazon's multi-million-square-foot facilities — contains tens of miles of conveyor belt and roller systems, operating at line speeds of up to 2.5 m/s, processing over **one million individual items per day**, fed by **robotic pod-retrieval systems** (the descendants of Kiva Systems' autonomous mobile shelving units, acquired by Amazon in 2012 and rebranded as **Amazon Robotics**), sorted by **high-speed crossbelt sortation systems** capable of processing over 20,000 items per hour at sort accuracies exceeding 99.99%, and discharged into **automated packing stations** where **collaborative robotic arms** equipped with **machine vision systems** place items into custom-dimensioned cartons selected automatically based on the item's scanned dimensions and weight. The entire system is orchestrated in real-time by a **Warehouse Control System (WCS)** that communicates simultaneously with hundreds of PLCs, motor drives, barcode scanners, vision systems, and robotic controllers across the facility, processing tens of thousands of control transactions per second to maintain the precise, synchronised material flow on which the facility's extraordinary throughput depends.

3.1.3 Classification of Industrial Conveyor Systems

Modern industrial facilities do not rely on a single type of conveyor; they deploy a highly integrated and strategically designed network of **specialized continuous transport mechanisms**, each selected on the basis of its optimized suitability for a specific combination of material characteristics, load geometry, operating environment, throughput requirement, and process integration demands. The primary engineering classifications are:

1. **Flat Belt Conveyors:** The most universally recognized and widely deployed conveyor type globally. It utilizes a continuous loop of synthetic material — typically multi-ply **polyester-nylon fabric** with **PVC, polyurethane, or rubber covers** — supported on a flat metal slider bed or closely spaced idler rollers and driven by a motorized head pulley. Flat belt conveyors are the default choice for transporting **irregularly shaped items**, **fragile or delicate goods**, **small discrete components**, and **bulk powders or fine granulates** that would fall through the gaps between the rollers of a roller conveyor. They are the universal standard in **airport check-in baggage handling**, **supermarket checkout**, **postal letter and flat mail processing**,

pharmaceutical tablet and capsule transport, and **electronics assembly**.

2. **Troughed Belt Conveyors:** The dominant technology for **bulk material handling** in mining, quarrying, cement, steel, power generation, and bulk port terminal operations. The belt is supported on **troughed idler sets** — typically three-roll sets at 20°, 35°, or 45° trough angles — which form the belt into a trough cross-section that dramatically increases volumetric carrying capacity. Modern troughed belt conveyors span individual flight lengths of up to **20 kilometers** on overland systems, carry belt loads of up to **30,000 tonnes per hour** on wide, high-speed mining conveyors, and operate at belt speeds of up to **10 m/s**. The steel-cord reinforced belt constructions described in the materials evolution section are standard on all high-capacity and long-distance troughed belt systems.

3. **Roller Conveyors:** Systems in which the payload is supported and conveyed by rolling contact against a series of closely spaced parallel cylindrical rollers mounted transversely across the conveyor frame, rather than by a continuous belt surface.

    - **Gravity Roller Conveyors:** Entirely unpowered systems installed on a slight downward gradient (typically 3–5°) that utilize the **gravitational potential energy** of the payload to provide the driving force for motion. They are the most energy-efficient conveyor type and are widely used for **carton flow racks**, **loading dock gravity lines**, and **decline transfer chutes** in warehousing and distribution. They require no power supply, no control system, and essentially no maintenance beyond periodic roller bearing lubrication.
    - **Powered (Live) Roller Conveyors:** Systems in which each roller is positively driven by a **motorized chain**, a **continuous flat belt** running beneath the rollers in contact with their undersides, or — in modern **Motor-Driven Roller (MDR)** systems — an individual **24V DC brushless electric motor** built directly inside the roller tube. MDR-powered roller conveyors represent the current state of the art in **zero-pressure accumulation conveying**, offering zone-by-zone independent speed control, extremely low energy consumption (each zone motor consuming only 50–100W), near-silent operation, and the ability to handle products ranging from lightweight polybags to heavy pallets on the same conveyor line.

4. **Modular Plastic Chain Conveyors:** Systems in which the carrying surface is constructed from interlocking, injection-molded thermoplastic segments (typically **acetal/POM**, **polypropylene**, or **polyethylene**) that form a continuous articulated conveying surface geometrically analogous to a tank tread. These systems are highly resistant to **aggressive chemical cleaning agents**, **high-pressure hot water wash-down** (up to 85°C), **UV radiation**, and **low-temperature freezer environments** (−40°C). They are the universally accepted industry standard in **food processing** (meat, poultry, seafood, bakery, confectionery, dairy, and fresh produce), **pharmaceutical bottling and blister packaging**, and **beverage filling and packaging** operations where rigorous **HACCP compliance** and hygienic design standards are mandatory.

5. **Overhead Conveyors:** Systems suspended from the facility ceiling or structural steelwork in which a continuous motorized drive chain running within an elevated **enclosed track profile** tows a series of **trolley carriers** fitted with hooks, fixtures, or hangers from which products, components, or assemblies are suspended. **Power-and-Free overhead conveyors** — in which individual carriers can be **selectively stopped, accumulated, diverted, and re-routed** independent of the main drive chain by means of mechanically or pneumatically actuated **dog clutch mechanisms** — are the dominant technology in **automotive body-in-white paint and surface treatment lines**, **general manufacturing assembly lines**, and **electroplating and heat treatment operations**.

6. **Screw Conveyors:** A continuously rotating helical screw blade (the **flight**) enclosed within a U-shaped trough or circular tube, descended directly in functional principle from the Archimedean screw of antiquity. Screw conveyors excel at the controlled, **enclosed, metered transport** of fine powders, granules, wet sludges, semi-solid pastes, and thermally sensitive bulk materials that would segregate, aerate, degrade, or spill unacceptably on a conventional belt or roller system. They are the standard for **flour and grain metering in bakeries**, **cement clinker and fly ash handling in concrete batching plants**, **sludge transport in wastewater treatment works**, **plastic pellet feeding to extruders**, and **pharmaceutical powder transfer between process vessels**. The completely enclosed construction of the tube-type screw conveyor also provides effective **dust containment** in environments where airborne powder is a health hazard, an explosion

risk, or a product contamination concern.

7. **Pneumatic Conveyor Systems:** Systems that use **differential air pressure** — either **positive pressure** generated by a blower at the inlet, or **negative pressure (vacuum)** generated by an exhauster at the outlet — to suspend and propel fine powder or granular materials as an **aerosol suspension** (in **dilute-phase conveying**) or as discrete **moving plugs** of densely packed material separated by air cushions (in **dense-phase conveying**) through closed, sealed **pipeline networks** that can route the material around bends, through walls and floors, and to multiple simultaneous destinations without any mechanical carrying element. Pneumatic conveyors are indispensable in **flour milling** (intra-mill flour transfer), **pharmaceutical active ingredient handling** (where product containment and cross-contamination prevention are regulatory requirements), **plastic pellet conveying from silos to processing machines**, and **cement and fly ash pneumatic transfer systems** in ready-mix concrete plants.

8. **Vibrating Conveyors:** Systems in which a material-carrying trough or deck is subjected to precisely controlled, **high-frequency, small-amplitude oscillatory motion** generated by **eccentric mass drives**, **electromagnetic coil actuators**, or **pneumatic vibrators**, causing granular or fragmented materials resting on the trough surface to advance along its length through **inertial micro-displacement** — each oscillation cycle imparting a small net forward momentum to the material through the asymmetric acceleration profile of the trough motion. Vibrating conveyors are preferred in applications handling **hot foundry castings** (where contact with rubber or plastic belt surfaces would cause thermal damage), **fragile food products** (where the gentle, consistent vibratory motion minimizes product breakage), **chemically aggressive bulk materials**, and applications requiring **simultaneous conveying and screening** (by mounting perforated deck sections to allow undersized fines to fall through during transport).

3.1.4 The Era of Automation and Cyber-Physical Integration (Industry 4.0)

The final evolutionary leap of the conveyor system — which directly defines the core engineering objective of this internship project — is the integration of digital logic, embedded systems, and **Cyber-Physical Automation**.

In the late 20th and early 21st centuries, passive mechanical belts were transformed into highly intelligent, autonomous routing systems. Driven by precision actuators such as **Stepper Motors** and **Servo Drives**, and monitored by continuous-feedback mechanisms such as **Optical Encoders**, **Ultrasonic Transducers**, and **Photoelectric Sensors**, the modern conveyor is no longer a "dumb" continuous loop. It is a **precision-controlled, data-generating, self-monitoring process system** that communicates continuously with upstream and downstream equipment, higher-level factory management software, and cloud-hosted analytics platforms.

A modern automated conveyor functions as an **intelligent node** within the **Industrial Internet of Things (IIoT)**. It possesses the computational capability to precisely count discrete objects, calculate real-time throughput rates, dynamically modulate its speed to prevent downstream bottlenecks, and pause with **millimeter precision** to allow for automated robotic arm manipulation. Embedded **vibration sensors** and **thermal imaging systems** continuously monitor the mechanical health of idler bearings and drive pulleys, feeding data to **predictive maintenance algorithms** that schedule component replacement before catastrophic failure occurs — eliminating the unplanned downtime that can cost large automated facilities tens of thousands of dollars per operating hour.

The integration of **Machine Vision Systems** — high-resolution industrial cameras coupled with **deep learning inference engines** — mounted above conveyor lines enables **100% automated quality inspection** of products at full production speed, detecting surface defects, dimensional deviations, color variations, label misplacements, and foreign object contamination with a consistency and statistical accuracy that no human inspector can sustain over an extended production shift.

It is exactly this critical intersection of raw **mechanical hardware** and sophisticated **microcontroller intelligence** that Phase 2 and Phase 3 of this internship project will explore, prototype, and mathematically validate.

3.2 Phase 2: Initial Prototyping and Mechanical Validation

With the theoretical framework of continuous transport established, the objective of Phase 2 was to construct a physical proof-of-concept. Rather than attempting a complex, bespoke fabrication immediately, this initial prototype was modeled after an existing open-source electromechanical design to validate the fundamental actuation and control logic before committing to heavy industrial materials.

3.2.1 Mechanical Architecture and Actuation Strategy

The structural foundation of the first iteration utilized a **Slotted Angle Iron Chassis**. This material was selected for its rapid-prototyping capabilities; the pre-drilled slots allowed for highly adjustable mounting of the drive components and idler rollers without requiring precision machining or welding.

To achieve the precise velocity control and high holding torque required for automated material handling, a **Hybrid Stepper Motor** was selected as the primary prime mover, managed by an **Industrial Microstepping Driver** (a high-amperage, discrete driver module). Unlike standard DC motors which require complex closed-loop encoder feedback for speed regulation, a stepper motor rotates in precise, discrete angular increments dictated by digital pulse trains from the microcontroller, allowing for exact volumetric throughput control.

Power transmission from the stepper motor shaft to the primary **Drive Pulley** was achieved utilizing a **Synchronous GT2 Timing Belt Drive**. By interlocking the toothed GT2 neoprene belt with corresponding aluminum timing pulleys, the design completely eliminated the risk of power-transmission slip between the motor and the drive roller, ensuring a 1:1 mechanical transfer of rotational torque.

3.2.2 Iteration 1: Elastic Belt Implementation

For the first iteration, the mechanical design was modeled closely after an established open-source reference architecture[1]. A 130 mm wide continuous band of highly compliant **Elastic Fabric** was stretched over the cylindrical head and tail rollers.

[1]Design reference based on external documentation: https://youtu.be/5sep7IT5YgA

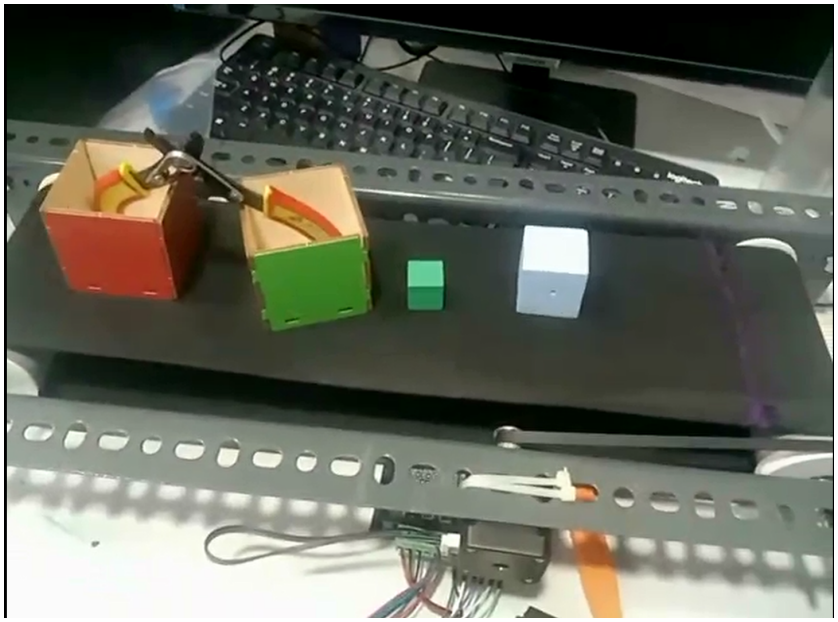

Figure 3.1: Phase 2, Iteration 1 prototype utilizing a slotted angle iron frame and a highly compliant elastic belt, based on an external reference design.

However, upon initial power-up and payload testing, two severe mechanical failure modes immediately manifested:

1. **Payload Sag (Deflection):** Because the elastic belt was suspended purely in tension between the two rollers without any underlying rigid support, the introduction of a physical payload caused severe localized downward deflection. The elastic material stretched under the gravitational force, creating a mechanical trough that stalled the motor and prevented linear transport.

2. **Lateral Belt Mis-tracking:** As documented during experimental observation, the belt refused to remain centered. Within seconds of actuation, the elastic band would aggressively slide laterally along the longitudinal axis of the rollers, eventually slipping entirely off the edge of the chassis and jamming the rotational mechanism.

3.2.3 Iteration 2: Material Upgrade and Slider Bed Integration

Hypothesizing that the high elasticity and lack of structural support were the primary causes of the mechanical failure, a mid-phase redesign was executed.

First, to resolve the payload sag, a rigid **Cardboard Slider Bed** was fabricated and mounted securely to the angle iron frame directly beneath the top strand of the belt. This converted the system from a pure roller-supported belt to a **Slider-Bed Conveyor**, allowing the belt to glide over a flat planar surface and enabling it to support significantly heavier discrete weights without vertical deflection.

Secondly, the highly compliant elastic belt was discarded and replaced with a **Rexine Sheet** (a synthetic artificial leather fabric). Rexine possesses a much higher tensile modulus and significantly lower elastic deformation under load, more closely mimicking the mechanical properties of an industrial PVC conveyor belt.

Figure 3.2: The Phase 2 prototype featuring the slotted angle iron chassis, the upgraded Rexine synthetic belt, and the integrated cardboard slider bed utilized to provide rigid vertical payload support.

3.2.4 Failure Analysis and Root Cause Identification

Following the Iteration 2 upgrades, the conveyor successfully transported the payload during the initial test cycles. However, under sustained continuous operation, the fatal flaw re-emerged: the Rexine belt began to exhibit the same **severe lateral mis-tracking**, eventually slipping off the head pulley.

Because the belt material had been upgraded to a non-elastic synthetic and the vertical sag had been eliminated by the slider bed, the root cause was analytically determined to be a fundamental flaw in the **Chassis Geometry**.

In conveyor engineering, belt tracking is overwhelmingly dictated by the **Parallelism** of the rotating shafts. For a flat belt to remain perfectly centered, the central axis of the drive pulley and the central axis of the tail

pulley must be geometrically parallel to a tolerance of fractions of a millimeter. If one side of the tail pulley is even slightly further away from the drive pulley than the other side, it creates an asymmetric tension gradient across the width of the belt. Physics dictates that a moving belt will inherently climb toward the side with the lowest tension.

The **Slotted Angle Iron Chassis** was the true point of failure. The inherent dimensional tolerances of the pre-drilled slots, combined with the lack of cross-bracing rigidity, made it physically impossible to lock the two roller shafts into perfect, immovable parallel alignment. Any vibration from the stepper motor caused micro-shifts in the frame geometry, instantly inducing lateral belt slip.

3.2.5 Conclusion of Phase 2

While the Phase 2 prototype ultimately failed as a reliable continuous transport mechanism, it was a highly successful engineering diagnostic exercise. It validated the GT2 synchronous power transmission and the microstepping actuation logic, but conclusively proved that a rapid-prototyping chassis cannot provide the strict geometric parallelism required for belt tracking.

To achieve a functional, automated industrial conveyor, Phase 3 required a total mechanical paradigm shift: discarding the slotted angle iron in favor of a rigid, custom-fabricated frame capable of enforcing strict geometric tolerances.

3.3 Phase 3: Final Mechanical Design and Integration

The analytical failure of the Phase 2 prototype conclusively demonstrated that a high-precision, continuous-transport mechanism cannot rely on structurally compliant framing materials. To resolve the fatal lateral mis-tracking caused by shaft misalignment, Phase 3 required a total mechanical paradigm shift toward high-rigidity materials and strictly enforced geometric tolerances.

The foundational architecture for this final iteration was inspired by an established open-source desktop conveyor model[2]. However, significant proprietary modifications were engineered to optimize the power-to-weight ratio, reduce reliance on oversized stepper motors, and integrate custom **Fused Deposition Modeling (FDM) 3D-printed** mechanical couplings.

3.3.1 Material Selection: 2020 Aluminum Extrusion Architecture

To categorically eliminate the parallelism failures inherent to the slotted angle iron, the chassis was completely reconstructed utilizing **2020 Series Aluminum T-Slot Extrusion Profiles (20x20mm)**.

The selection of T-slot aluminum provided immediate, critical structural advantages:

- **Absolute Orthogonality:** By utilizing precision-cast 90-degree internal **Corner Brackets**, the longitudinal frame rails and vertical support legs were locked into perfect right angles. This guaranteed that the lateral distance between the left and right rails remained identical across the entire length of the conveyor bed.
- **Infinite Linear Adjustability:** The continuous T-slots allowed the 3D-printed bearing holders to be slid smoothly along the rails before being torqued down. This enabled micro-millimeter adjustments to the belt tension (**Take-up Actuation**) without the stepped limitations of pre-drilled holes.
- **High Torsional Rigidity:** The internal webbing of the 2020 profile resists twisting forces (torsion) caused by uneven payload weight, keeping the slider bed perfectly horizontal.

[2]Base mechanical architecture inspired by open-source documentation: https://www.printables.com/model/745444-mini-conveyor/files

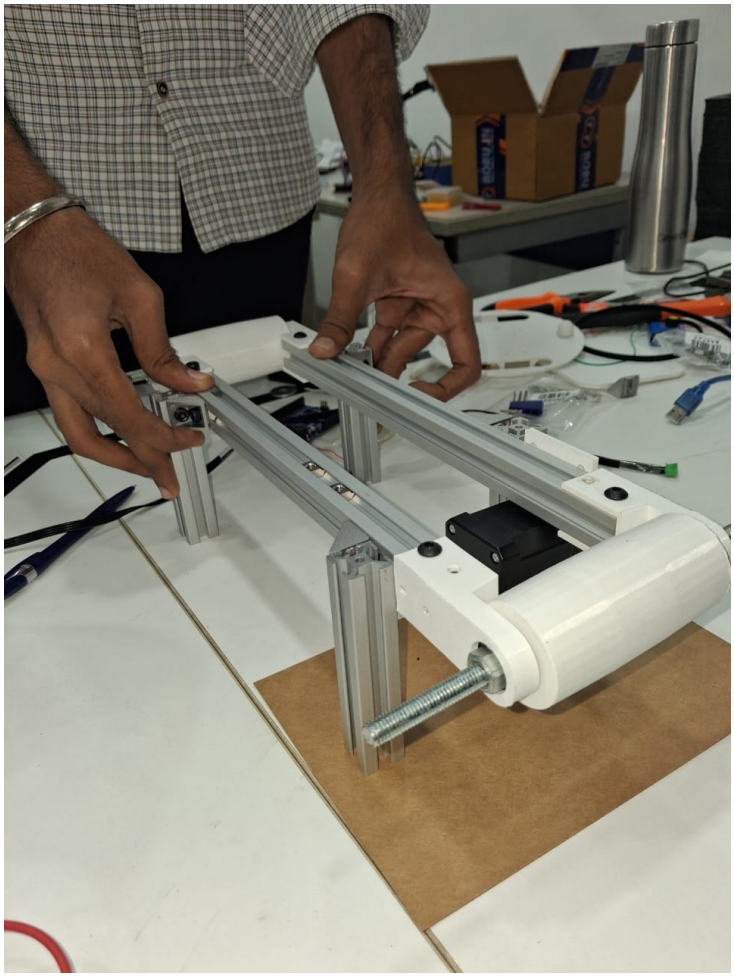

Figure 3.3: Manual assembly of the Phase 3 chassis, demonstrating the structural rigidity of the 2020 aluminum extrusions and the integration of the 3D-printed bearing holders and head pulley.

3.3.2 System Bill of Materials (BOM)

The complete mechanical and electromechanical integration required a hybrid approach, combining off-the-shelf industrial hardware with custom rapid-prototyped polymers. The comprehensive Bill of Materials is detailed in Table 3.1.

Table 3.1: Phase 3 Conveyor System Comprehensive Bill of Materials

Category	Component Description	Quantity
3D Printed Models	Drive/Tail Roller Cylinders	2
	608RS Bearing Holder Mounts	4
	8mm Shaft Holder	1
Aluminum (2020 T-Slot)	300mm Longitudinal Extrusion	2
	100mm Vertical/Transverse Extrusion	6
	M4 Button Head Screws	30
	M4 T-Slot Nuts	30
	90-Degree Corner Brackets	8
Electromechanical & Hardware	BO Geared DC Motor (100 RPM)	1
	Continuous Synthetic Belt	1
	608RS Sealed Ball Bearings	4
	M8 Threaded Rod/Bolts (125mm)	2
	M8 Hex Nuts	5
	Nylon Zip Ties	1

3.3.3 Actuation Redesign: Direct-Drive BO Motor and Custom Coupling

The reference open-source design utilized a heavy NEMA 17 stepper motor coupled to the drive roller via an external GT2 timing belt and pulley system. Upon analyzing the required throughput and anticipated payload mass for this specific prototype, it was determined that a NEMA 17 motor was severely over-specced, adding unnecessary weight, electrical complexity, and cost.

An engineering decision was made to substitute the stepper motor with a lightweight, highly efficient **100 RPM BO (Battery Operated) Geared DC Motor**. The internal dual-axis gearbox of the BO motor provides substantial torque at a low rotational velocity, making it ideal for continuous, steady-state material transport.

The "Inner Join" Custom Shaft Coupling

Because the NEMA 17 and timing pulleys were discarded, a new method for transmitting torque directly from the BO motor to the 3D-printed drive roller was required. The BO motor features a highly specific dual-flat, slotted plastic output shaft, which does not naturally mate with a standard cylindrical roller.

To resolve this, a proprietary **Internal Spline Coupling** (colloquially referred to as an "Inner Join") was designed utilizing CAD software.

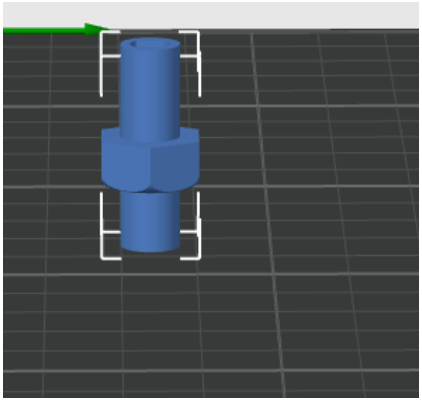

Figure 3.4: CAD rendering of the proprietary "Inner Join" coupling, engineered to directly mate the dual-flat BO motor shaft with the internal geometry of the 3D-printed drive roller.

This custom 3D-printed adapter was engineered with female geometries on one end to grip the BO motor shaft tightly without slipping, and a male hexagonal/cylindrical geometry on the opposing end to press-fit seamlessly into the hollow core of the 3D-printed drive roller. This achieved a highly efficient **Direct-Drive transmission**, eliminating the external GT2 belt entirely and dramatically reducing the mechanical footprint of the system.

3.3.4 Roller Mechanics and Bearing Integration

To ensure the friction between the spinning rollers and the stationary chassis was minimized, **608RS Sealed Deep-Groove Ball Bearings** were integrated into the design.

- **Dead-Shaft Configuration:** The 125mm M8 bolts function as stationary "dead shafts" passing through the 3D-printed bearing holders.
- **Rotational Freedom:** The 608RS bearings sit inside the ends of the 3D-printed rollers, allowing the plastic cylinder to spin effortlessly around the stationary M8 bolt. This drastically reduced the required starting torque (F_i) demanded from the BO motor.

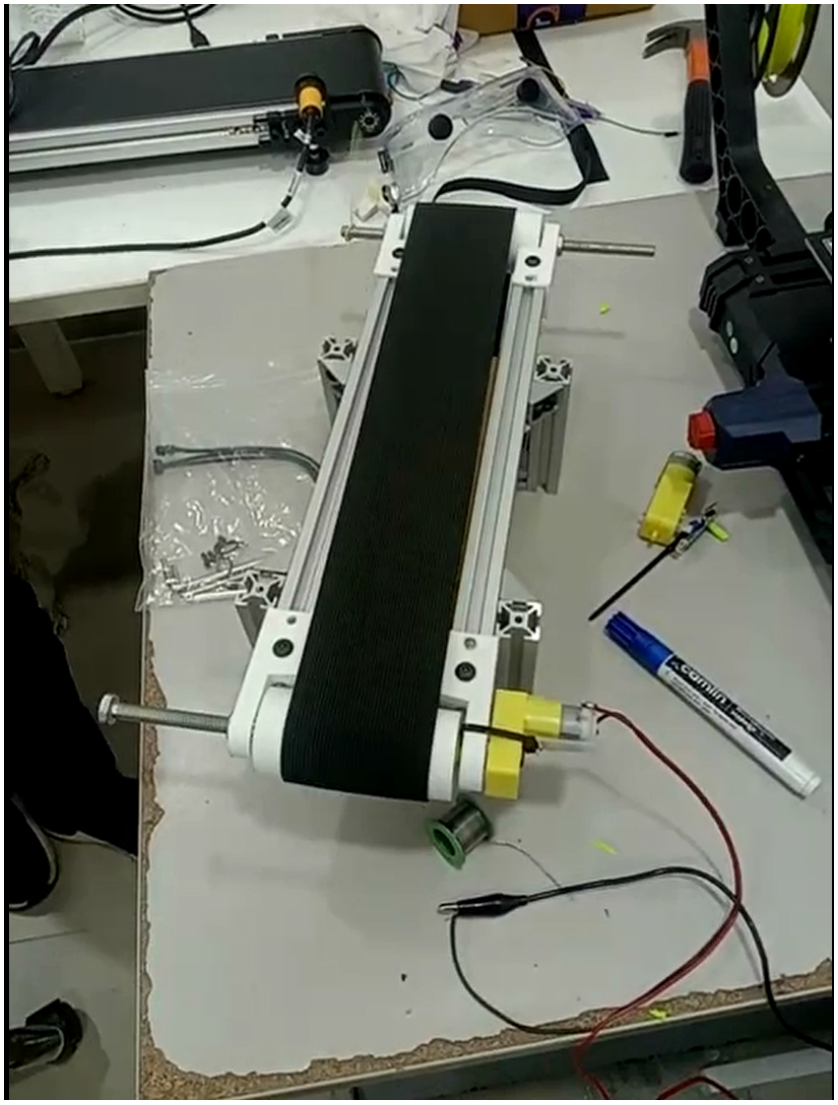

Figure 3.5: The fully assembled Phase 3 automated conveyor, featuring the taut synthetic belt, 2020 aluminum structural frame, direct-drive BO motor, and M8 dead-shaft bearing integration.

3.3.5 Electrical Control and Experimental Validation

With the mechanical architecture finalized and absolute shaft parallelism achieved, the final stage involved electrical validation. Two specific experiments were conducted to verify the control logic and the physical efficiency of the mechatronic system.

Experiment 1: Variable Velocity Control via Potentiometer

In industrial settings, conveyors must dynamically adjust their speed to prevent downstream bottlenecks. To simulate this, a 10kΩ rotary potentiometer was integrated into an Arduino microcontroller circuit.

The Arduino's 10-bit ADC read the analog voltage gradient from the potentiometer (0–1023). A custom firmware script utilized the `map()` function to translate this input into an 8-bit Pulse Width Modulation (PWM) signal (0–255). This PWM signal was fed through a motor driver to the BO motor. As the operator rotated the potentiometer, the duty cycle of the motor dynamically scaled, demonstrating perfectly smooth, continuous acceleration and deceleration of the payload belt without stalling.

Experiment 2: Back-Electromotive Force (EMF) Generation

To scientifically validate the extremely low rolling resistance of the 608RS bearings and the reversibility of the DC motor's magnetic field, a unique mechanical experiment was performed. The power supply to the BO motor was disconnected, and an LED was wired directly across the motor's terminals.

By manually pulling the conveyor belt, the human operator provided kinetic energy to the system. The mechanical rotation of the belt spun the drive roller, which in turn back-drove the gearbox and spun the armature of the BO motor inside its permanent stator magnets. According to **Faraday's Law of Induction**, this relative motion generated a **Back-Electromotive Force (Back-EMF)**:

$$V_{emf} = K_e \cdot \omega$$

Where V_{emf} is the generated voltage, K_e is the motor's specific voltage constant, and ω is the angular velocity of the armature. The manual actuation of the belt generated sufficient electrical voltage to successfully illuminate the LED. This experiment proved two things: the DC geared motor can function as a highly efficient alternator, and the aluminum/bearing chassis possesses so little frictional resistance that manual actuation can easily overcome the gearbox ratio.

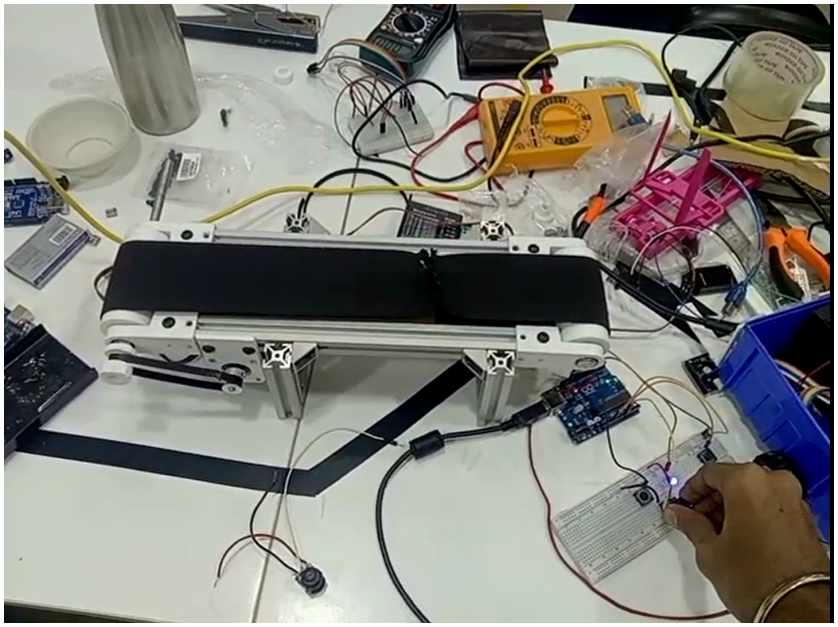

Figure 3.6: Electrical validation and control testing, demonstrating the Arduino-based potentiometer variable speed circuit and the Back-EMF generation experiment.

3.3.6 Conclusion of the Conveyor Project

The Phase 3 rebuild was an absolute engineering success. By applying rigorous structural mechanics (2020 extrusions) and custom 3D-printed direct-drive actuation, the fatal flaws of belt mis-tracking and payload deflection were entirely eliminated. The resulting mechanism is a robust, variable-speed, continuous transport platform fully capable of interfacing with discrete robotic systems such as the AGV.

Chapter 4

Internship Outcomes and Conclusion

4.1 Comprehensive Learning Outcomes

The one-month FOSSEE (Free/Libre and Open Source Software for Education) Winter Internship at the Indian Institute of Technology (IIT) Bombay provided an intensive, hands-on proving ground that successfully bridged the critical gap between theoretical academic concepts and applied industrial mechatronics. The development of both the Automated Guided Vehicle (AGV) and the Automated Conveyor System yielded profound technical and methodological learning outcomes across multiple engineering disciplines:

4.1.1 Embedded Systems and Firmware Engineering

- **Microcontroller Architecture Management:** Developed a rigorous understanding of 8-bit AVR microcontroller constraints (specifically the ATmega328P). Learned to optimize C++ firmware to execute complex floating-point calculus without exceeding the highly limited 2 KB Static RAM (SRAM) boundary.
- **Hardware Abstraction and Signal Processing:** Mastered the programmatic translation of raw physical phenomena into actionable digital logic. This included continuous analog-to-digital (ADC) sensor data normalization and the generation of high-frequency Pulse Width Modulation (PWM) signals for variable-speed motor actuation.

4.1.2 Applied Control Theory and Kinematics

- **Discrete-Time Calculus Implementation:** Successfully translated continuous-time mathematical models into discrete-time software algorithms. Most notably, implemented and empirically tuned a Proportional-Integral-Derivative (PID) control loop to achieve stable, high-speed line tracking, moving beyond primitive binary control logic.

- **Differential Drive Kinematics:** Gained practical expertise in translating abstract steering correction variables into physical wheel velocities, utilizing dynamic braking and asymmetric motor reversing to negotiate sharp radii under payload inertia.

4.1.3 Mechanical Design and Iterative Prototyping

- **Structural Rigidity and Material Science:** Learned the critical importance of material selection through physical failure analysis. The analytical transition from a compliant slotted angle-iron frame to high-rigidity 2020 Aluminum T-Slot extrusions provided firsthand experience in resolving complex kinematic failures, specifically lateral belt mis-tracking caused by millimeter-scale shaft misalignment.

- **Rapid Manufacturing and CAD:** Developed high proficiency in Computer-Aided Design (Autodesk Fusion 360) and Fused Deposition Modeling (FDM) 3D printing. Engineered and successfully deployed custom electromechanical interfaces, such as the proprietary "Inner Join" direct-drive motor coupling and dead-shaft bearing housings.

4.1.4 Electromechanical Diagnostics and Professional Methodology

- **Empirical Physics Validation:** Conducted physical experiments to validate theoretical laws, including Back-Electromotive Force (EMF) generation and Faraday's Law of Induction, proving the reversibility of the DC gear motor assembly and the low frictional resistance of the mechanical chassis.

- **The Open-Source Engineering Paradigm:** Internalized the FOSSEE methodology of utilizing open-source hardware (Arduino) and software libraries to rapidly prototype industrial-grade solutions, radically reducing development costs while maintaining high functional reliability.

4.2 Conclusion

The primary objective of this internship was to explore, design, and empirically validate the core mechatronic components of modern industrial material handling. By successfully engineering both a discrete transport platform (the Automated Guided Vehicle) and a continuous transport mechanism (the Automated Conveyor System), this objective was conclusively achieved.

These rigorous development cycles explicitly demonstrated the intricate, unforgiving dependencies between mechanical integrity, electrical power distribution, and algorithmic intelligence. The systemic failures encountered during the early prototyping phases—such as the AGV's payload limitations on an acrylic chassis and the conveyor's belt slip on a structurally compliant frame—served as invaluable, hands-on engineering lessons that textbook theory alone cannot adequately convey.

Ultimately, the rigorous, iterative design methodology championed by the FOSSEE project has profoundly enhanced my practical engineering capabilities as a Computer Engineering student. The systems engineered during this month stand as robust, scalable prototypes, successfully demonstrating the foundational principles of Industry 4.0, and setting a firm intellectual foundation for future academic research in autonomous robotics, machine vision, and cyber-physical systems.

Bibliography

[1] Microchip Technology Inc., *ATmega328P 8-bit AVR Microcontroller with 32K Bytes In-System Programmable Flash Datasheet*, Rev. A. Chandler, AZ: Microchip Technology, 2018.

[2] STMicroelectronics, *L298 Dual Full-Bridge Driver Datasheet*, Rev. 6. Geneva, Switzerland: STMicroelectronics, 2000.

[3] Vishay Semiconductors, *TCRT5000 / TCRT5000L Reflective Optical Sensor with Transistor Output Datasheet*, Rev. 1.8. Malvern, PA: Vishay Intertechnology, 2009.

[4] Pololu Corporation, *Micro Metal Gearmotor Specifications and Performance Data*. Las Vegas, NV: Pololu Robotics and Electronics, 2021.

[5] Panasonic Corporation, *NCR18650B Rechargeable Lithium-Ion Battery Product Specifications*. Osaka, Japan: Panasonic Automotive & Industrial Systems Company, 2012.

[6] Conveyor Equipment Manufacturers Association (CEMA), *Belt Conveyors for Bulk Materials*, 7th ed. Naples, FL: CEMA Publications, 2014.

[7] K. Ogata, *Modern Control Engineering*, 5th ed. Upper Saddle River, NJ: Prentice Hall, 2010.

[8] A. Kumar and S. Singh, "Design and Development of Automated Guided Vehicle with Line Follower Concept using IR," *2023 Fifth International Conference on Electrical, Computer and Communication Technologies (ICECCT)*, Veladas, India, 2023, pp. 1-6.

[9] Z. Wang, "OpenCV-based PID Control Line Following Vehicle with Object Recognition and Reaction," *AIP Conference Proceedings*, vol. 3085, no. 1, 2024.

[10] J. Smith and L. Chen, "Dynamic Modeling and Tracking Control of Industrial Belt Conveyor Systems," *IEEE Transactions on Industrial Electronics*, vol. 65, no. 8, pp. 6421-6430, Aug. 2018.

[11] M. Hermann, T. Pentek, and B. Otto, "Design Principles for Industrie 4.0 Scenarios," *2016 49th Hawaii International Conference on System Sciences (HICSS)*, Koloa, HI, USA, 2016, pp. 3928-3937.